Atmospheric Rivers as Triggers of Compound Flooding: Quantifying Extreme Joint Events in Western North America Under Climate Change

Andrew Vincent Grgas-Svirac[1], Mohammad Fereshtehpour[1], M. Reza Najafi[1], Alex J. Cannon[2], Hamidreza Shirkhani[3]

[1]Department of Civil and Environmental Engineering, University of Western Ontario, London, Canada.
[2]Climate Research Division, Environment and Climate Change Canada, Victoria, BC, Canada.
[3]National Research Council Canada, Ottawa, ON, Canada

Corresponding author: M.R. Najafi (mnajafi7@uwo.ca)

Abstract. Atmospheric Rivers (ARs) are narrow bands of concentrated moisture that transport water vapor from the tropics to higher latitudes. They are responsible for ~90% of poleward water vapor transport and play a vital role in water resource management along the North American west coast. While ARs significantly contribute to regional water supplies, they are also major drivers of flooding. This study investigates the extent to which ARs contribute to compound inland flooding (CIF) events where multiple drivers intensify flood risks, namely Rain on Snow (ROS) and Saturation Excess Flooding (SEF) events. Furthermore, the influence of anthropogenic climate change is investigated relative to internal climate variability. Using the CanRCM4 Large Ensemble simulations, we analyze the frequency and seasonality of AR-driven CIF events in Western North American coastal areas, with emphasis on interactions between ARs and antecedent snowpack and soil moisture. ARs are found to be dominant drivers of CIF events by contributing to the development and intensification of these events. These conditions also shape the seasonality and intensity of AR-driven CIFs. Projections suggest that internal climate variability can significantly contribute to future uncertainty in CIF frequency and intensity, complicating efforts to predict and mitigate these events. The findings underscore the importance of integrating AR-related flooding risks into flood management strategies and infrastructure design to adapt to a changing climate.

1. Introduction

Atmospheric Rivers (ARs) are synoptic-scale phenomena characterized by long, narrow bands of concentrated water vapor that transport moisture from tropical and subtropical regions to higher latitudes. They frequently form in association with

extratropical cyclones and are a key driver of heavy precipitation and flooding in mid latitude regions (Ralph et al., 2017, 2020). Unlike other large scale moisture transport mechanisms, such as cut-off lows and synoptic scale frontal systems, ARs frequently transport an intense amount of moisture inland (Mishra et al., 2025). Despite only occupying about 10% of space on the globe at a given time, they are estimated to be responsible for 90% poleward water vapor transport across the mid latitudes (Ralph et al., 2020; Zhu & Newell, 1998). Along coastal regions in the mid latitudes, ARs play an important role in local water resource management, often serving as primary contributors to annual precipitation. This is particularly evident during the autumn and winter seasons along the North American west coast, where ARs deliver the majority of precipitation and significantly influence regional hydrology (Lamjiri et al., 2018; Rutz et al., 2014). In the State of California, the majority of annual precipitation has been found to be associated with a few very strong AR related winter storms (M. Dettinger, 2016; M. D. Dettinger et al., 2011). AR related precipitation contributes significantly to both rainfall and snowfall. At higher elevations and in colder regions, they are key providers of snow pack that can act as natural reservoirs to support seasonal water resource availability for agricultural, ecological, and urban needs (Guan et al., 2010, 2016; Rutz et al., 2014). Studies in British Columbia indicate that ARs contribute approximately 90% of annual extreme precipitation, and account for more than 33% of annual total precipitation (Sharma & Déry, 2020a). Similar findings have been reported for landfalling ARs in Southwest Alaska, where ARs also play a dominant role in extreme precipitation events (Nash et al., 2024; Sharma & Déry, 2020a).

Landfalling AR storms deliver substantial precipitation that often provide beneficial impacts, such as drought relief and reservoir replenishment. In California alone, 74% of droughts have ended upon the arrival of an AR (Dettinger, 2013). However, the intense precipitation brought by ARs also act as a driving force of flooding events. In the western United States, ARs are one of the primary causes of flooding. For example, in California's Russian River Basin all major floods between 1997 and 2006 have been attributed to landfalling ARs (Ralph et al., 2006). Comprehensive studies of the entire U.S. west coast have shown that a large portion of annual runoff peaks are associated with AR occurrence (Barth et al., 2017; Konrad & Dettinger, 2017). In British Columbia's coastal region, research indicates that for many watersheds, up to half of annual streamflow is linked to landfalling ARs (Sharma & Déry, 2020b). Furthermore, one of the most severe flooding events in the province's history occurred when two ARs made landfall in November 2021. The result was widespread infrastructure failure due to flooding and landslides, with damages totalling 65 million CAD, the displacement of 20 000 residents and five deaths (Gillett et al., 2022; Richards-Thomas et al., 2024). Most recently, in October 2024, a strong AR made landfall in BC, delivering 150–300 mm of rain, which overwhelmed metropolitan storm sewers resulting in widespread flooding (Cassidy, 2024). Overall, substantial evidence links severe flooding in North America's west coastal regions to landfalling ARs.

Given their ability to deliver large amounts of precipitation rapidly, ARs often amplify the severity of flooding events when combined with other contributing factors. This makes ARs a significant driver of compound inland flooding (CIF) events, where multiple mechanisms interact to produce extreme runoff. A compound event is defined as an event with amplified severity due to the contribution of multiple drivers or hazards (Hao & Singh, 2020; IPCC, 2012; Zscheischler et al., 2020). Examples of compound flooding events include Rain on Snow (ROS) and Saturation Excess Flooding events (SEF). An ROS

event occurs when intense rainfall falls on snowpack generating large amounts of snowmelt, amplifying runoff generation. SEF events occur when soil is saturated prior to an intense rainfall event, leading to an amplified runoff response due to the lack of infiltration. Soil saturation can arise from various moisture sources, however, ARs have the potential to be a key driver because of their dominant role in large-scale, intense moisture transport. Recent high-profile catastrophic AR-related flooding events indicate that although ARs often act as primary drivers of extreme precipitation, the resultant runoff response is frequently amplified by pre-existing conditions such as saturated soils or snowmelt. For example, the extreme runoff generated in February 2017, which led to the failure of the Oroville Dam spillway, was driven by a combination of unusually deep antecedent snowpack undergoing rapid melting, high antecedent soil moisture and the arrival of an AR storm (Henn et al., 2020). Similarly, during the November 2021 British Columbia floods, ARs were identified as the primary driver with a large portion of the impact attributed to snowmelt which amplified the runoff response (Gillett et al., 2022). These flooding events involved multiple contributing factors, including AR-driven precipitation combined with antecedent conditions such as snowmelt and saturated soils emphasizing the complex interactions that often modulate CIF events. Most AR-related studies focus primarily on the extreme precipitation or runoff generated by individual landfalling AR events and often overlook the compounded effects of multiple drivers. This gap in understanding can lead to an underestimation of the overall hazard (Singh et al., 2021; Wazneh et al., 2020). The importance of considering the dependence between multiple drivers in relation to AR events is underscored by previous studies, which show that even lower-intensity ARs can generate significant runoff when combined with factors such as saturated soils or snowmelt (Chen et al., 2019; Konrad & Dettinger, 2017).

In a warming climate, AR events are generally projected to become more frequent and intense (Gonzales et al., 2019; O'Brien et al., 2022; Radić et al., 2015; Shields et al., 2023), which is expected to exacerbate flooding conditions in regions that regularly experience AR-driven events. In the previously discussed regions, several studies have already explored the potential impact of more frequent and intensified AR events under future warming scenarios. Current evidence suggests that projected changes in AR characteristics are likely to result in more frequent and severe flooding events along the North American West Coast. In California the projected changes in AR may result in large increases in AR-related extreme precipitation and the elevated risk of flooding events (Gershunov, et al., 2019; Huang & Swain, 2022; Shields et al., 2018). Furthermore, projected changes in landfalling ARs are also associated with projected increases in fiscal flood losses relative to the historical period (Huang & Swain, 2022; Rhoades et al., 2021). In British Columbia, streamflow and extreme precipitation are projected to increase in proportion to the increase in AR related activity (Curry et al., 2019). Similar trends have been identified for AR activity in Alaska, with projections indicating corresponding increases in extreme precipitation and runoff (Nash et al., 2024). Furthermore, several studies suggest that under a warming climate, the frequency of sequential AR events is expected to increase, further amplifying the future risk of AR-related flooding events (Bowers et al., 2023, 2024; Fish et al., 2022). Although AR storms are recognized as significant contributors to ROS and SEF events (Guan et al., 2016; Ralph et al., 2013; Rhoades et al., 2024; Shulgina et al., 2023), most existing AR studies primarily focus on extreme precipitation and its immediate impacts. While there have been a few regional studies examining AR interactions with ROS events and snow accumulation (Guan et al., 2010; Kim et al., 2013), there is a critical gap in understanding the broader role of ARs in compound

flooding events. Existing work that explicitly addresses atmospheric river–driven compound inland flooding remains limited (Bowers et al., 2024; Ridder et al., 2018). This lack of research on the interaction between ARs and multiple drivers, such as SEF and ROS, may lead to an underestimation of their amplified role in future compound flooding, especially under a warmer climate where such interactions could become more frequent and impactful.

This study quantifies the contribution of ARs to compound inland flooding by investigating the co-occurrence probability of landfalling ARs, extreme precipitation and CIF events such as ROS or SEF along western North American coastal areas. Western North America has been chosen due to its historic vulnerability to AR related flooding events, as highlighted in previous studies. We also investigate the influence of seasonality on the frequency and intensity of these joint occurrences. Furthermore, recognizing the growing evidence linking an increase in AR occurrence to a warming climate, we evaluate the role of anthropogenic climate change and internal climate variability in AR-induced compound flooding under different warming levels. While previous research has primarily focused on ROS and AR on the U.S. side of the Pacific Northwest or specific case studies (Bowers et al., 2024; Guan et al., 2016; Rhoades et al., 2024), our study offers a novel perspective by examining how ARs contribute to both ROS and SEF as compound flooding mechanisms in a broader inland context. This dual focus allows us to assess the role of ARs in driving these mechanisms and to evaluate how their influence may shift under future climate scenarios using the CanRCM4 large ensemble simulations. Section 2 describes the datasets and methods employed. Section 3 presents the results, and Section 4 discusses the findings in the context of existing literature.

2 Methodology

2.1 Climate Data

The study employs the Canadian Regional Climate Model Large Ensemble (CanRCM4-LE) that covers North America at a resolution of 0.44° x 0.44° (~ 50 km). CanRCM4 is driven by the second generation Canadian Earth System Model (CanESM2) large ensemble, using historical forcing from the Coupled Model Intercomparison Project Phase 5 (CMIP5) for 1950–2005 and Representative Concentration Pathway (RCP) 8.5 forcing from 2006 to 2100 (Scinocca et al., 2016; Singh et al., 2021). To effectively characterize compound events, a large sample of events is essential for a robust statistical analysis (Zscheischler and Seneviratne, 2017). This study utilizes 28 members from the CanRCM4-LE model to analyze compound events, ensuring a robust statistical assessment. The selection of 28 members aligns with previous studies, which have successfully characterized AR-related events using ensembles of similar size (Hagos et al., 2016; Michaelis et al., 2022; Tseng et al., 2022). Each ensemble member includes daily simulations of integrated vapor transport (IVT), precipitation, snowmelt, and soil moisture from 1950 to 2100. In this study, CanRCM4 is re-gridded to the 0.5° rectangular grid using bilinear interpolation with land cells considered in the following analysis (Figure 1). The data was re-gridded to facilitate future comparisons to bias corrected CanRCM4 datasets (Cannon et al., 2022), however, the simulations analyzed here are not bias corrected.

The CanRCM4-LE dataset was generated by perturbing the initial conditions of the individual model, allowing for the characterization of internal climate variability. Since the differences between ensemble members arise solely from these initial

condition perturbations, rather than variations in model structure, the approach isolates the effects of internal variability (Deser et al., 2020; Kay et al., 2015). To improve estimates of nonstationary extreme statistics, the large ensemble treats all simulations as approximately statistically independent, given the model's sensitivity to atmospheric initial conditions (Haugen et al., 2019; Stein, 2020; Tebaldi et al., 2021). Previous studies have demonstrated that CanRCM4 performs well in reproducing key regional climate patterns relative to observed data (Il Jeong and Cannon, 2020; Whan and Zwiers, 2016). Furthermore, the model has been shown to represent AR activity with acceptable accuracy (Whan and Zwiers, 2016). To further validate the CanRCM4-LE dataset to represent AR activity, it will be evaluated against the ERA5 reanalysis dataset during the baseline period. ERA5, developed and maintained by the European Centre for Medium-Range Weather Forecasts (ECMWF), is a global reanalysis dataset that provides a continuous and consistent record of atmospheric variables (Hersbach et al., 2020). ERA5 has been shown to reasonably capture AR activity (Collow et al., 2022) and is widely used in similar studies for AR analysis (Espinoza et al., 2018; Guan and Waliser, 2019; Lavers and Villarini, 2015; Rutz et al., 2014; Tseng et al., 2022). In terms of AR detection, ERA5 generally resembles observational satellite data with a slight positive (negative) bias in higher(lower) latitude regions (Cobb et al., 2021; Ma et al., 2023). For comparison, hourly IVT data from ERA5 is aggregated into daily values and re-gridded to a 0.5° × 0.5° rectangular grid to align with the resolution of the CanRCM4-LE dataset.

This study presents projections at four warming levels using 31-year time frames: the Baseline (BL) period (1986-2016) corresponding to a +1 °C global mean temperature change (GMTC) compared to the pre-industrial level (1850-1900), WL1.5 (2001-2031) corresponding to +1.5 °C GMTC, WL2 (2013-2043) corresponding to +2 °C GMTC, and WL4 (2053-2083) corresponding to +4 °C GMTC (Cannon et al. 2020). For regional interpretation, the Bukovsky regions, as shown in Figure 1a are considered. These regions offer a simplified representation of North America's terrestrial ecoregions, serving as a useful proxy for identifying areas with similar climatological characteristics (Bukovsky, 2011). Figure 1a also shows the approximate location of dams within the region, obtained from the Global Dam Tracker database, providing insight into potential impacts on infrastructure (Zhang and Gu, 2023). Figure 1b depicts approximate elevation of the area as a point of reference while discussing results since topography plays an important role in AR related events. Elevation data was processed from the Global Multi-resolution Terrain Elevation Data 2010 (GMTED 2010) dataset created by USGS during the shuttle radar topography mission (Danielson and Gesch, 2011).

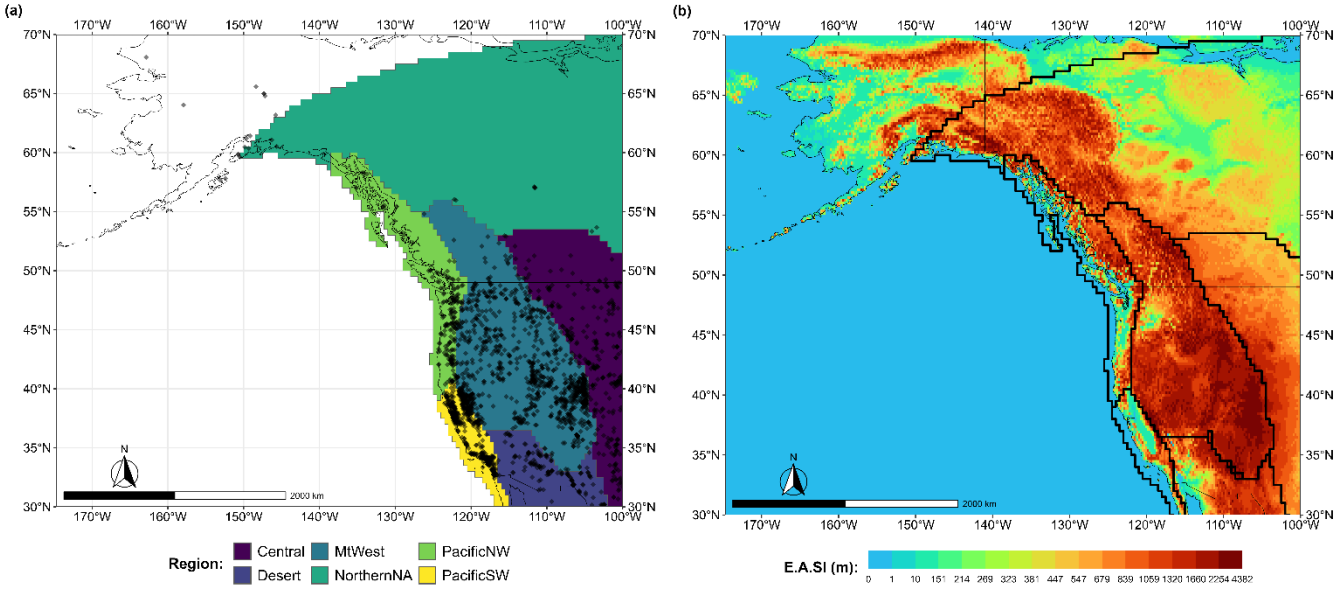

Figure 1: Study area, a) subdivided by Bukovsky regions with the black diamonds indicating the reservoir locations from the Global Dam Tracker database, b) the approximate Elevation Above Sea level (EASl) in meters at a resolution of 0.22°x0.22° from the GMTED 2010 dataset provided by USGS.

2.2 AR Detection

ARs are identified using the Eulerian perspective developed by Ralph et al. (2019), which detects ARs using integrated vapor transport over time. The Eulerian perspective is a widely used approach that defines an AR as an observer would at a specific location monitoring conditions over time (Guan and Waliser, 2015; Rutz et al., 2014). The Eulerian perspective is selected for this study since it optimizes the balance between computational efficiency across multiple members and physical realism in the scope of the current work. Furthermore, it allows to consistently link moisture transport extremes to flood events across the study domain without introducing additional complexity from object-based AR detection methods. In this study, AR conditions are defined for a single cell in which IVT exceeds 250 kg/m/s for over 24 hours (1 day) according to the scaling provided by Ralph et al. (2019). A limitation of this approach is that the spatial structure of atmospheric rivers is not explicitly represented. However, object-based detection criteria were found to offer limited additional benefit for the objectives of this study, which focus on temporal coincidence rather than spatial geometry. Previous work has shown that point-based threshold methods can detect AR activity with acceptable performance, particularly in coastal regions and in regional climate model simulations where full AR object detection may be less reliable (Guan et al., 2023). To further assess the performance of the chosen point based threshold method, a sensitivity analysis with ERA5 data was conducted, comparing the threshold-based method to the algorithm of (Guan and Waliser, 2019), and the TEMPEST algorithm (Ullrich et al., 2021). A fixed IVT threshold of 250 kg/m/s is often considered at the minimal IVT threshold in AR studies for this region (Chen et al., 2019; Gershunov et al., 2017; Radić et al., 2015; Ralph et al., 2019a, b; Rutz et al., 2014; Sharma and Déry, 2020a, b). A sensitivity

analysis using the chosen detection technique, (Figure S1), indicates that detected AR activity is consistent across the study area is robust against changes in IVT threshold. Detailed regional and seasonal calibration of detection thresholds is beyond the scope of this study and will be addressed in future work. Recognizing that weak to moderate ARs can have significant impacts, these thresholds align with ARs that are primarily category 1 or higher to allow for a wide range of AR events to be considered. For example, the AR associated with the 2021 British Columbia floods had a return period of just 10 years but the associated 2 day rainfall had a 50 to 100 year return period (Gillett et al., 2022). Because rainfall intensity is more closely linked to total moisture convergence, most atmospheric river detection methods do not always fully capture the intensity of AR-related storms, as they are primarily based on the magnitude of moisture transport rather than precipitation processes (Mo et al., 2021).

2.3 CIF Event Definition and Likelihood

This study considers the likelihood of two different types of CIF events coinciding with a landfalling atmospheric river. Each type of CIF event is identified using a threshold definition of their respective drivers. The percentile-based approach takes advantage of the large amount of data provided by the large ensemble and avoids model biases (Poschlod et al., 2020). Each quantile threshold is calculated based on the time series for each individual grid cell, ensuring each threshold reflects extremes at local climatology. The CIF events defined in this study are ROS events and SEF events. A high threshold is used to ensure the most severe events are identified. ROS events are identified when daily precipitation and snowmelt exceed the 98th percentile simultaneously within a single grid cell. In addition, snowmelt should contribute to at least 20% of the combined liquid generated during the event to ensure that ROS events detected in the CanRCM4 dataset are impactful, rather than instances with no snowmelt or when snowmelt is negligible. Days without meaningful snowmelt are automatically excluded by the 20% snowmelt-contribution threshold, so that non-snow-season precipitation does not generate false ROS detections. This threshold is a conservative estimate for ROS events based on the approximate amount of snowmelt contribution identified in observational results (Freudiger et al., 2014; Musselman et al., 2018). While this approach may exclude some physically plausible but less extreme ROS events, such as moderate, persistent rainfall on snow, it is appropriate for this study because the objective is to characterize the most consequential events rather than the full ROS climatology. SEF events are defined as days when both daily precipitation and soil moisture exceed their respective 98th percentiles. Soil moisture within CanRCM4 is updated based on cumulative infiltration and evapotranspiration from previous days, therefore the daily soil moisture values effectively represent antecedent soil conditions. The likelihood of Extreme Precipitation (XPRA) Events coinciding with landfalling atmospheric rivers are also considered to further contextualize CIF likelihood. XPRA events are defined as days when 1-day precipitation exceeds the 98th percentile. The 98th-percentile thresholds are computed per grid cell to reflect local climatology, and previous sensitivity testing (Fereshtehpour et al., 2025) demonstrated that varying the percentile range (95th–99th) yields consistent spatial patterns, supporting the robustness of this choice. For all identified extreme precipitation, ROS,

and SEF events, surface runoff must exceed its 98th percentile on the same day or the day immediately afterward to account for short lags between rainfall and meltwater response in daily data. This additional criterion ensures that the events analysed are strongly linked to significant runoff generation and is consistent with typical hydrologic response times at a daily temporal resolution. It should be noted that a sensitivity analysis by Fereshtehpour et al. (2025) showed that incorporating event-based definitions with varying gap-day criteria (0–3 days) did not significantly alter the spatial patterns of CIF events, thereby supporting the robustness of the daily co-occurrence approach for the large-scale statistical analysis used in this study.

Events are defined as AR-related if they co-occurred with the pre-defined AR conditions described in Section 2.2. Most hydrological impacts from AR related precipitation is commonly associated with a 24-hour window (Chen et al., 2019; Oakley et al., 2017; Sharma and Déry, 2020a), which is also supported by case studies of impactful events (Gillett et al., 2022; Michaelis et al., 2022; Ralph et al., 2006). Accordingly, this definition minimizes the risk of decoupling atmospheric river occurrences from their associated hydrological impacts. Once all CIF events are identified for the study area, the conditional probability of an event being AR-related is calculated as the total number of identified AR related events divided by the total number of events. This represents the likelihood of a CIF event being associated with an AR, given the occurrence of a CIF event (Equation 1). To assess the significance of these probabilities for future projections, a bootstrapping method is applied. A single process variable, in this case rainfall, is randomly reshuffled 1000 times. The shuffled dataset is used to calculate a shuffled probability of occurrence for each CIF and XPRA event. The original and shuffled probabilities are compared using a two-sided t-test with a standard significance level of 0.05. Since the goal of this test is to determine whether the projections are created through random chance, the two-sided t-test is used to compare the means between the projected and randomly generated dataset. Since this procedure is used for each cell in the data set, the probability of a null hypothesis being falsely rejected during the analysis of the results is high. To mitigate the risk of overstating results, the procedure suggested by Wilks, 2016 is used to limit the false detection rate. This procedure creates a more sensitive null hypothesis threshold based on rank, number of tests, and a set control level for false detection rate. Assuming the results are spatially autocorrelated, a control level for false detection is set to two times the standard significance level (0.1) (Wilks, 2016).

$$\Pr(CIF|AR) = \frac{AR \cap CIF}{CIF} * 100\% \quad \text{(Eq. 1)}$$

Each type of CIF event is characterized by calculating the frequency and magnitude of each detected event. Frequency of a CIF event is calculated as the total sum of events that occurred in each month. The magnitude of the CIF event refers to the total volume of surface runoff produced during the event itself or the day following it. Surface runoff is used as a measure of magnitude since it is a more direct indicator of flooding potential compared to rainfall alone. The average frequency and magnitude across all 28 members are used as a representation of the general trend associated with CIF events, while the standard deviation across all 28 members is used as a representation of internal climate variability (ICV). The magnitude of CIF events without an AR present is also calculated (i.e., as non-AR event) to help contextualize the magnitude of the AR related CIF events.

3. Results

3.1 Evaluation of AR detection in CanRCM4-LE versus ERA5

To evaluate how well the CanRCM4-LE IVT outputs represent AR activity, the average number of ARs detected over the 31-year baseline period is calculated for each grid in both datasets. The CanRCM4-LE results are based on the 28-member ensemble mean. AR activity is expressed as the percentage of days within the 31-year period during which an AR occurs. AR activity detected in CanRCM4 compared to ERA5 is shown in Figure 2. Figure 2a considers the distribution of AR days in each region to show how well CanRCM4 represents AR activity relative to ERA5. Results indicate that CanRCM4 has a positive IVT bias in northern areas and a negative bias in southern areas. The positive bias is strongest in the PacificNW and Northern NA regions. The negative bias is strongest in the Desert region. Additionally, the central region displays higher positive biases in the dataset relative to the ERA5 and is a clear outlier. Despite these regional variations, the CanRCM4 distribution generally falls within the distribution detected in the ERA5 dataset. To examine how the general distribution of AR days changes over the whole study area, the average AR days was plotted with respect to latitude band in Figure 2b. The overall difference between the CanRCM4-LE and observational reanalysis is low ranging from 0 to +/- 2.5%. These results also further highlight the apparent positive bias in results for northern regions and negative bias in southern regions.

Additionally, a small-scale sensitivity test with ERA5 data was conducted to assess the robustness of the chosen AR detection technique relative to other commonly used algorithms, Guan and Waliser and Tempest. The result of this analysis is shown in Figure 3. This figure compares two generally accepted algorithms, TEMPEST and the Guan and Waliser algorithm, with the point-based threshold used in the study. The point-based threshold method shows broadly consistent regional patterns when compared to the other methods despite differences between each algorithm.

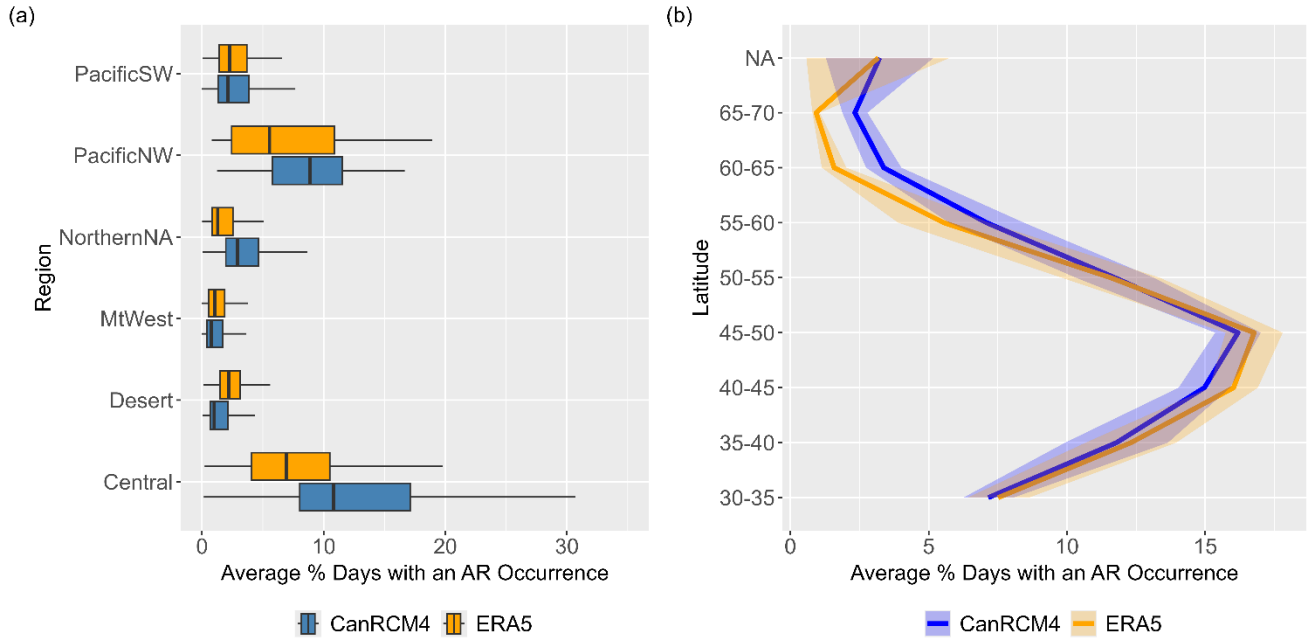

255

Figure 2: Average AR occurrence in the Baseline Period (1986-2016) expressed as the overall percentage of AR days detected in the 31-year period for CanRCM4 and ERA5 models. The distribution of days in each region is shown in a), while the latitudinal average for each model over the entire study area is summarized in b) with the average spread in the results.

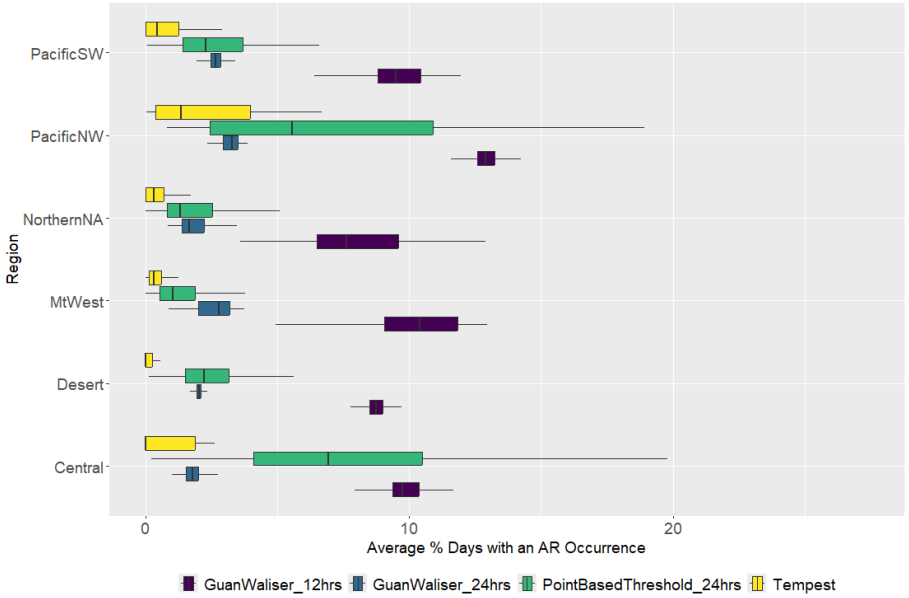

260 **Figure 3: Average AR occurrence in the Baseline Period(1986-2016) expressed as the overall percentage of AR days detected in the 31-year period for ERA5. The distribution of days detected in each region in the current study is compared for the Guan and Waliser algorithm results represent ARs counted on a daily and sub daily scale.**

3.2 Probability of Occurrence of a CIF being related to AR

To show the role ARs play in CIF events, the probability of an AR contributing to a CIF event is plotted spatially over the study area for each CIF event and warming level in Figure 4a. Additionally, spatially averaged probabilities by latitudinal bands are presented in Figure 3b to provide a broader perspective. Figure 4 displays results from the baseline period and WL4, and the projections for all warming levels are included in Figure S2. These results show that ARs play a major role in most CIF events specifically in coastal and midlatitude regions. This is especially significant when considering the overall likelihood of CIF occurrence in relation to extreme runoff, as shown in Figure S3. The increases in likelihood of AR contribution to CIF events (Figure S2) mirror the increases in overall likelihood of CIF occurrence (Figure S3) highlighting the importance of ARs in CIF events.

The PacificNW region emerges as the most active area, with at least 90% or more CIF events attributed to AR activity in each cell. Projections indicate that ARs can have an increasing impact in a warmer climate, as seen in the gradual expansion of high probability areas across warming scenarios. As shown in the line plots at different latitudinal bands, AR contribution to CIF events is projected to steadily increase between warming periods. These projections are spatially consistent for SEF and XPRA events, however, spatial changes in Figure 3a suggest that for ROS events the biggest changes in likelihood occur in higher elevation areas. For example, the MtWest region, characterized by higher elevations as shown in Figure 1b, is projected to experience an expansion in areas with a high likelihood of AR-related events. This aligns with findings from previous studies, which suggest that warmer climates may shift ROS events to higher altitudes (Il Jeong and Sushama, 2018; Musselman et al., 2018; Warden et al., 2024). It is important to note that in warmer climates, the statistical significance of projections decreases for ROS and SEF events, as shown by the reduction in stippling in the corresponding figures. This suggests that while ARs continue to play a significant role in extreme ROS and SEF events, these events may become less frequent or more challenging to statistically detect under future warming scenarios. In contrast, XPRA events maintain higher statistical significance across warming levels, reflecting their more consistent occurrence. Despite this decrease in statistical significance, ARs remain critical drivers of ROS and SEF events, particularly in regions such as the PacificNW and MtWest. This is especially important considering Figure 1a which shows this projection affects a large portion of the dam infrastructure on the West Coast. The high likelihood in the PacificNW region in all event types stands out from the other regions. This high activity can be attributed to this region containing most of the coastline in the study area and high elevation areas (see Figure 1b) which are both conducive to AR related storms.

The latitudinal distribution of ROS and SEF events shown in Figure 4b peaks between 45°N and 55°N, with a secondary peak at 60°N–65°N. The first peak corresponds to high-probability areas overlapping with the PacificNW and MtWest regions, where ARs penetrate furthest inland after landfall (Rutz et al., 2015). The secondary peak corresponds to an area of coastal Alaska not completely covered by the Bukovsky regions. In further regional breakdowns of the results this area will be referred

to as the Western Alaska region. In contrast, XPRA events show a different latitudinal pattern, with a single peak occurring between 45°N and 50°N and declining further northward. In these peak regions ARs contribute heavily to ROS and SEF events, and in some cases nearly all ROS and SEF events are AR-related. While XPRA events share some similarities, the overall probability of occurrence is lower, but the results exhibit higher statistical significance. This indicates that ARs may play less of a role in XPRA than CIF events. The second main difference is XPRA events show a different latitudinal pattern, with a single peak occurring between 45°N and 50°N and declining further northward. On the spatial maps this peak matches where ARs penetrate furthest inland as discussed previously.

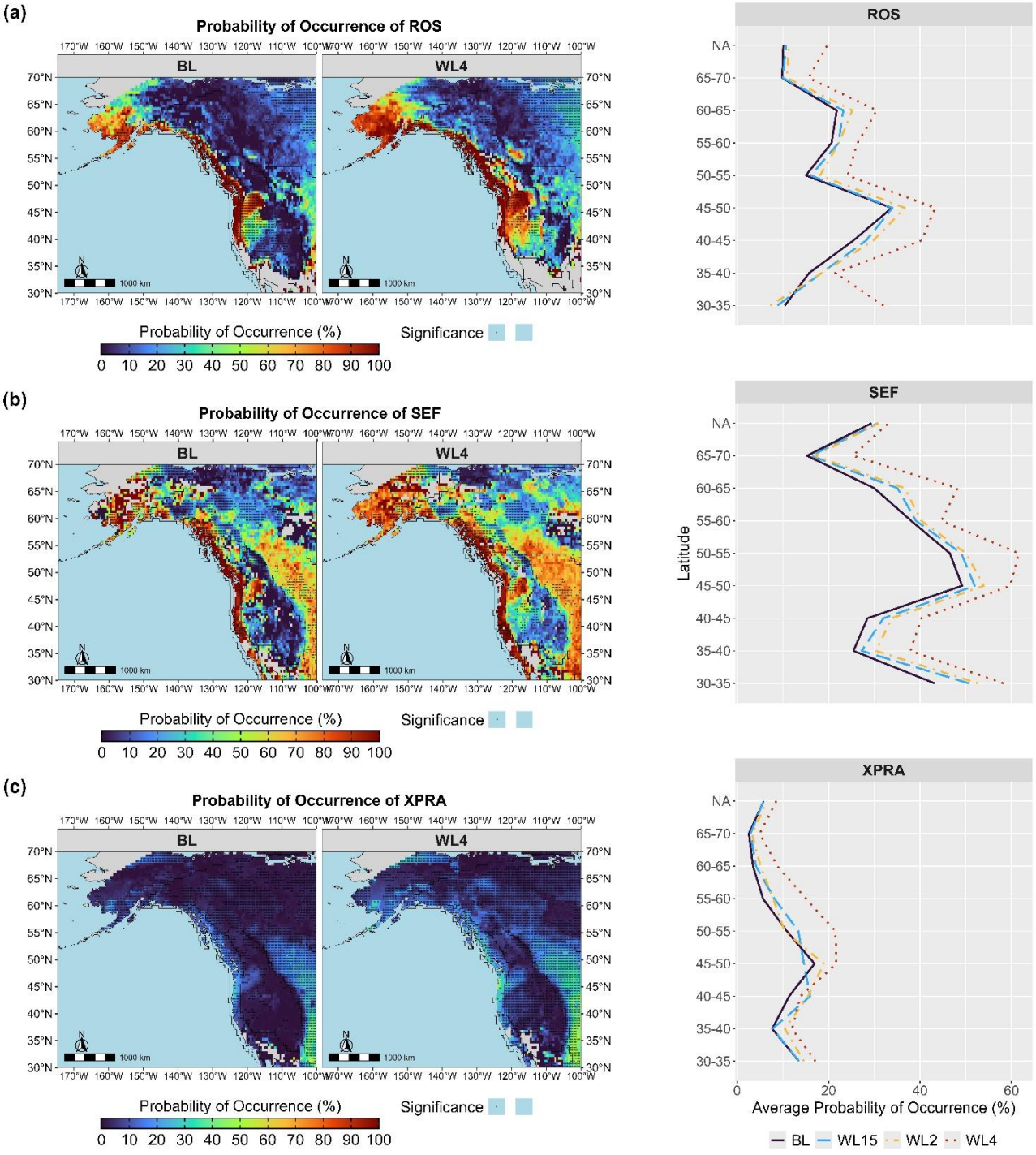

Figure 4: Spatial plot of probability of occurrence of an AR event given that ROS, SEF and XPRA events are occurring, in the BL (left) and WL4 (right) periods. Statistically significant results are represented by areas with stippling. The line plots depict the spatial average of probability of occurrence for each latitudinal band and CIF event.

3.3 Examining the Magnitude and Seasonality of AR related CIF Events

In this section we examine the magnitude and seasonality of AR related CIF events. Figures 5-7 display the spatial average magnitude using bar plots in terms of rainfall, snowmelt and runoff (mm) generated for each AR related events, and events without AR influence. The spatial average is weighted to account for the distortion of different latitudes. The value displayed on the bar chart is a ratio calculated as the mean magnitude of AR related events divided by the mean magnitude of regular events as a means of comparing the two scenarios. To further support these results, each cell with a non-zero magnitude is used to generate a kernel density plot for the study region in each season. This is to compare how likely a certain magnitude of an AR related event is relative to the likelihood of the magnitude of a regular event.

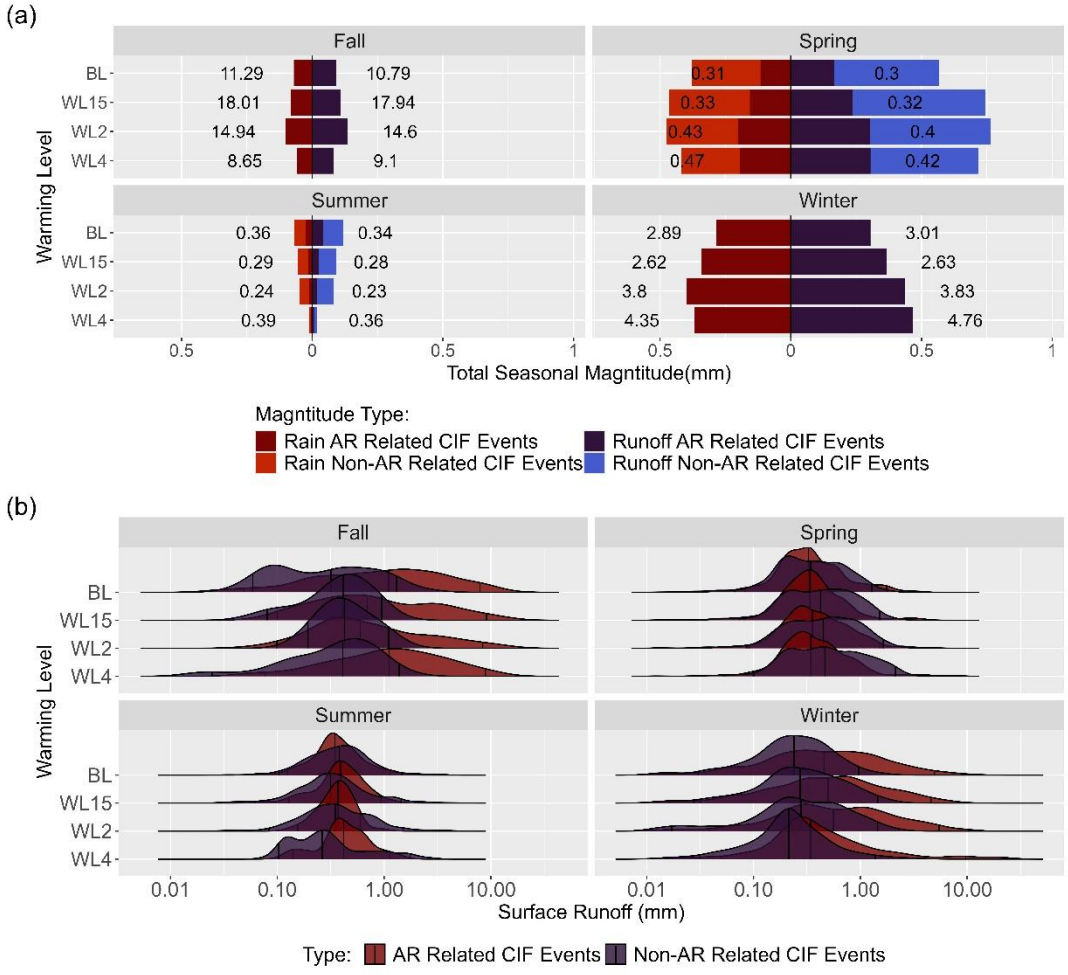

Figure 5: Seasonal magnitude for ROS events. a) proportion of magnitude between AR and non-AR events for each warming level in terms of precipitation (blue) and surface runoff (red). The values associated with each bar indicate the ratio of AR events to non-AR related events as a more objective measure of the difference in magnitude. b) probability of magnitude expressed as surface runoff for each warming level for AR related events (red) and non-AR related events(blue).

Figure 5a shows that ARs are most influential in ROS events during the Fall and Winter months where they are shown to be stronger by a large factor relative to non-AR events. However, unlike the probability of occurrence results, the magnitude is not projected to increase consistently over time in any season except winter. Instead, there is a projected increase until WL2 and then a projected decrease. This projection is reflective of other studies (Il Jeong and Sushama, 2018; Musselman et al., 2018) that also project increases in the frequency of ROS events in near term warming periods before decreasing in frequency in far term warming periods. The rainfall amounts shown in blue reveal that changes in rainfall generally reflect any increases or decreases in runoff magnitude. The kernel density plot for ROS events shown in Figure 5b shows that AR related ROS events are more likely to have higher median and extreme magnitudes than regular ROS events especially in the Winter and Fall. AR related ROS events are projected to be more likely stronger than regular events in future warming periods, as signified by the upper and lower quantiles moving further to the right for all seasons, further supporting that ARs continue to contribute to the highest magnitude ROS events.

Unlike ROS events, Figures 6 and 7 show that SEF and XPRA events are projected to consistently increase in magnitude with each warming scenario for all seasons. However, ARs contribute differently to each event. Figure 6a shows that the ratio of mean AR SEF magnitude to mean non-AR SEF magnitude is high during seasons with peak AR activity. Whereas ROS varied more seasonally, SEF magnitude is consistently projected to increase regardless of season, and by WL4, AR related SEF events are projected to be stronger relative to regular events in most seasons except Spring. However, the difference between AR related and regular events seems to decrease over time relative to the baseline period in terms of both generated rainfall and runoff. This could be indicative of non-AR related events also becoming more extreme parallel to AR events. However, the projections still show that AR related SEF events remain stronger than regular events in future warming scenarios. The distribution graph in Figure 6b shows that AR related events are generally more likely to be higher in magnitude relative to regular events in all seasons and warming periods. In a warmer climate AR related CIF events are more likely to have higher median and extreme runoff magnitudes in all seasons indicated by a right ward shift in all distributions.

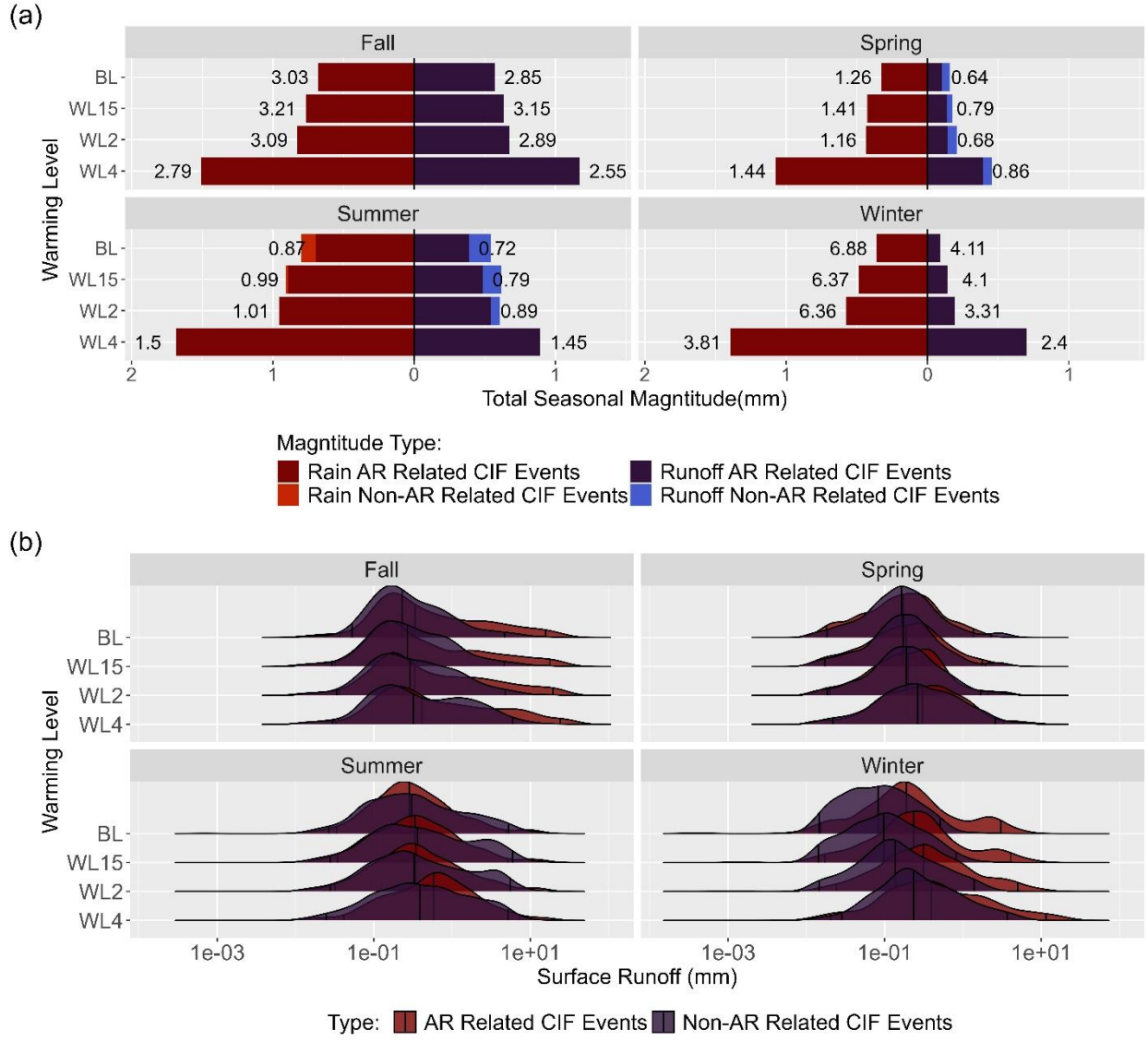

345

Figure 6: Seasonal magnitude for SEF events. a) proportion of magnitude between AR and non-AR events for each warming level in terms of precipitation (blue) and surface runoff (red). The values associated with each bar indicate the ratio of AR events to non-AR related events as a more objective measure of the difference in magnitude. b) probability of magnitude expressed as surface runoff for each warming level for AR related events (red) and non-AR related events(blue).

350 The XPRA results are unique from the other two CIF events, since the projected runoff of AR related XPRA events is not as strong as the ROS and SEF events. This could be reflective of the results in section 3.2 which show that ARs contribute less to XPRA related flooding and supports the projected importance of precedent conditions in AR related flooding. This is shown

in Figure 7a, in which the displayed ratios for each category are very low relative to the CIF events discussed previously. Furthermore, the kernel density plots in Figure 7b indicate for most seasons, the runoff generated by AR related extreme precipitation can be expected to be lower. Despite these findings, Figure 7a also shows that the projected magnitude of XPRA events increase over time indicating that, like the CIF events, AR related extreme precipitation is also projected increase in severity in a warmer climate.

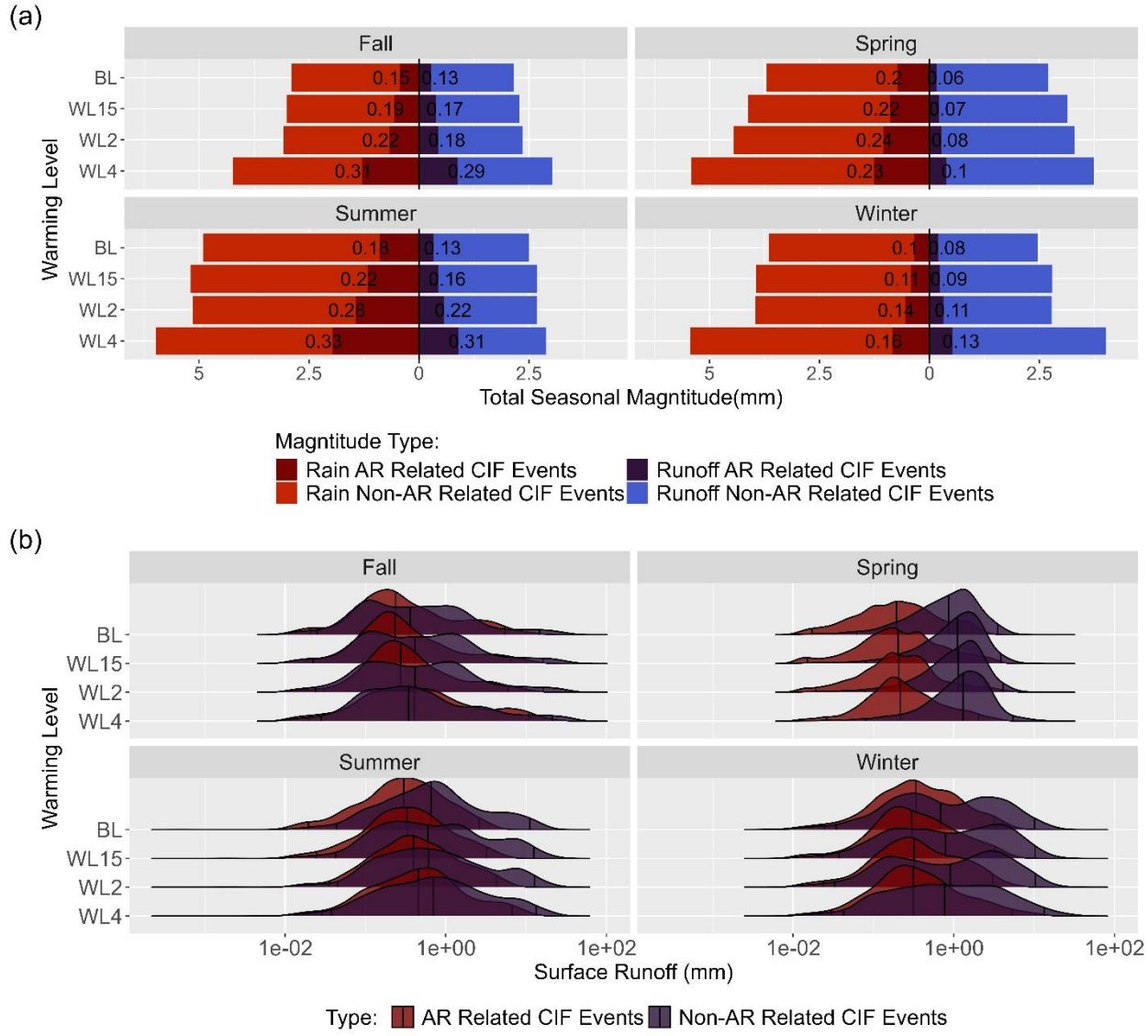

Figure 7: Seasonal magnitude for XPRA events. a) proportion of magnitude between AR and non AR events for each warming level in terms of precipitation (blue) and surface runoff (red). The values associated with each bar indicate the ratio of AR events to non AR related events as a more objective measure of the difference in magnitude. b) probability of magnitude expressed as surface runoff for each warming level for AR related events (red) and non-AR related events(blue).

For a more in-depth analysis of the contributions of snowmelt, rainfall and runoff during AR related ROS events, the projected average rainfall and snowmelt on days of identified ROS events are plotted in a bar chart with the average runoff in Figure 8. This compares the approximate proportional contribution of snowfall and rainfall to ROS runoff. The change in the ratio of snowmelt to rainfall relative to the baseline period is plotted against event frequency in Figure 9 to further explore this relationship. Figure 8 shows that, in general, changes in runoff across regions correspond proportionally to changes in the magnitude of rainfall and snowmelt associated with each event. Contrary to the expected decrease in snowmelt contribution in WL4, some regions may exhibit an increase in snowmelt contribution in the furthest projection. A notable example is the PacificNW region in winter, where the substantial increase in runoff likely skews the results in Figure 5a, leading to an apparent overall increase in winter event magnitude. Further examination of the PacificNW winter results suggests that this increased average may be driven by a rise in event frequency rather than a shift in the relative contribution of snowmelt, which remains largely consistent with the baseline period. When comparing Figures 8 and 9, it becomes evident that regions experiencing an increase in runoff by WL4 also see an increase in event frequency, whereas regions with decreased runoff exhibit a corresponding decline in frequency. These findings are explored in depth relative to past studies in the following discussion of results.

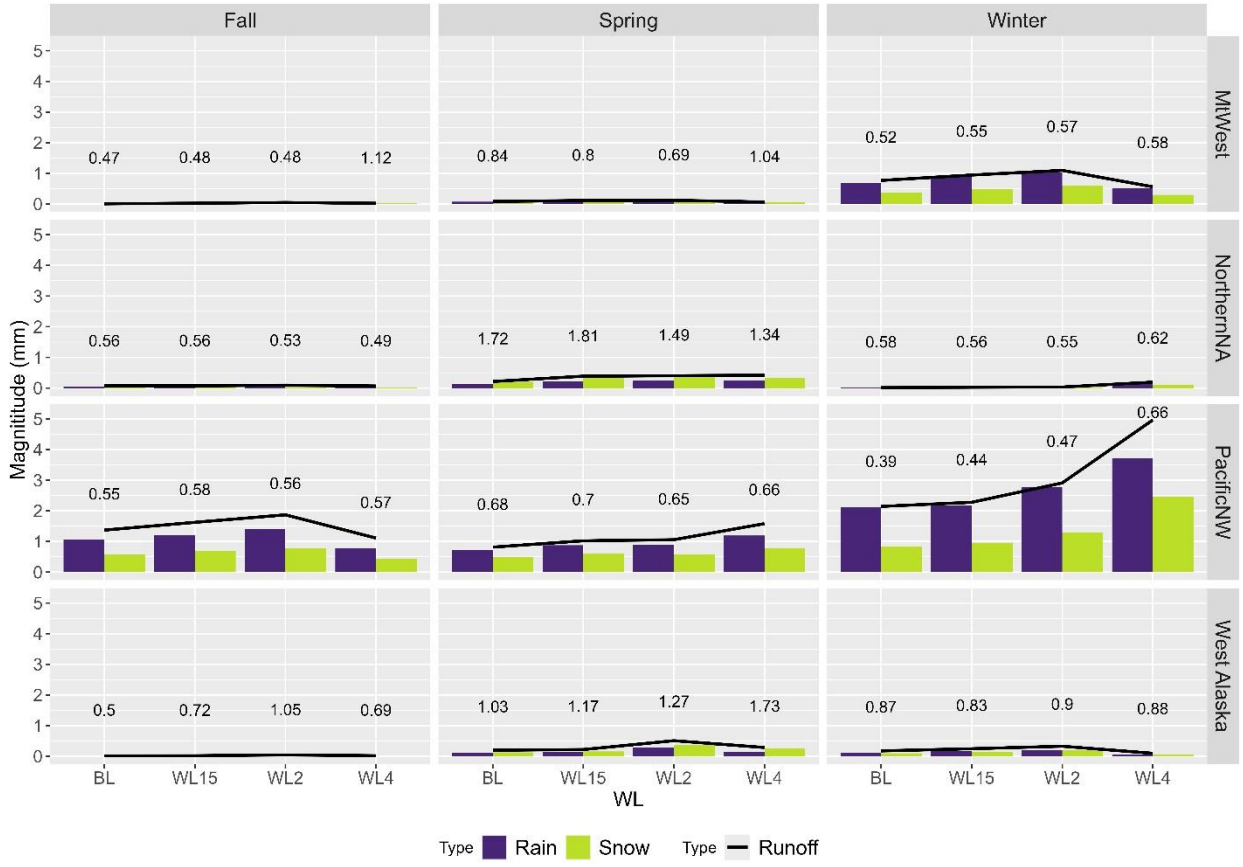

380

Figure 8:The spatial average of AR related ROS event magnitude expressed in terms of millimetres of runoff, rainfall and snowmelt generated on the day of the event for each season and region. The left, middle and right columns depict results from fall, spring, and winter respectively. From the top, the first, second, third and fourth rows depict the MtWest, NorthernNA, PacificNW and West Alaska regions respectively.

385

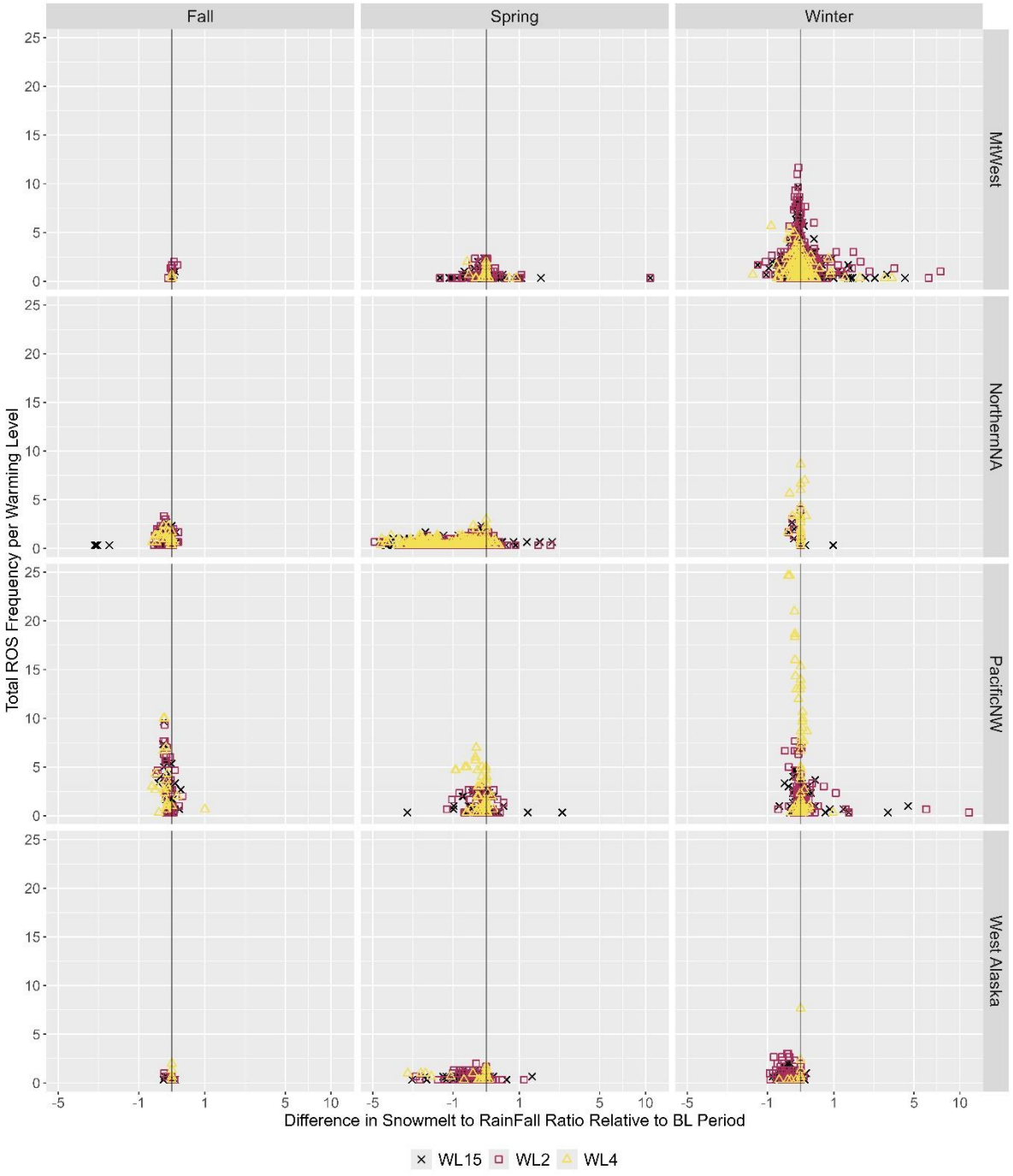

Figure 9: The regional and seasonal difference in snowmelt to rainfall ratio for WL15 ,WL2, and WL4,relative to the baseline period versus ROS event frequency at each grid point. The left, middle and right columns depict results from fall, spring, and winter respectively. From the top, the first, second, third and fourth rows depict the MtWest, NorthernNA, PacificNW and West Alaska regions respectively. The black line in the center of each plot marks zero.

To further examine regional seasonality, the month that contained the highest magnitude AR related event in terms of runoff is identified for each cell and plotted spatially in Figure 10. The findings in this figure support the results discussed above related to seasonality. For ROS events, the maps in the furthest warming period show that high impact events are projected to be more concentrated in winter seasons relative to the baseline period, especially in higher latitude areas. The results show a spatially homogenous projection which indicates ROS events will mainly occur in Winter in future warming scenarios. The seasonality of SEF and XPRA share a regional dependence that is unique relative to the ROS seasonality. Figure 10 clearly shows that northern regions experience AR related events in the fall while southern regions experience them in the winter. Furthermore, this seasonality remains consistent in the projected warming scenarios. Generally, these results show that during peak AR seasons ROS and SEF events on average have a higher magnitude than non-AR events. However, it is noted that changes in ROS events seem to be more closely related to factors such as elevation and snowpack levels. Furthermore, AR related CIF events are projected to be more likely and severe extremes. The difference in magnitude can largely be attributed to the increase in rainfall brought by a landfalling AR as indicated by the changes in precipitation results. This indicates that high runoff response is highly dependent on antecedent conditions.

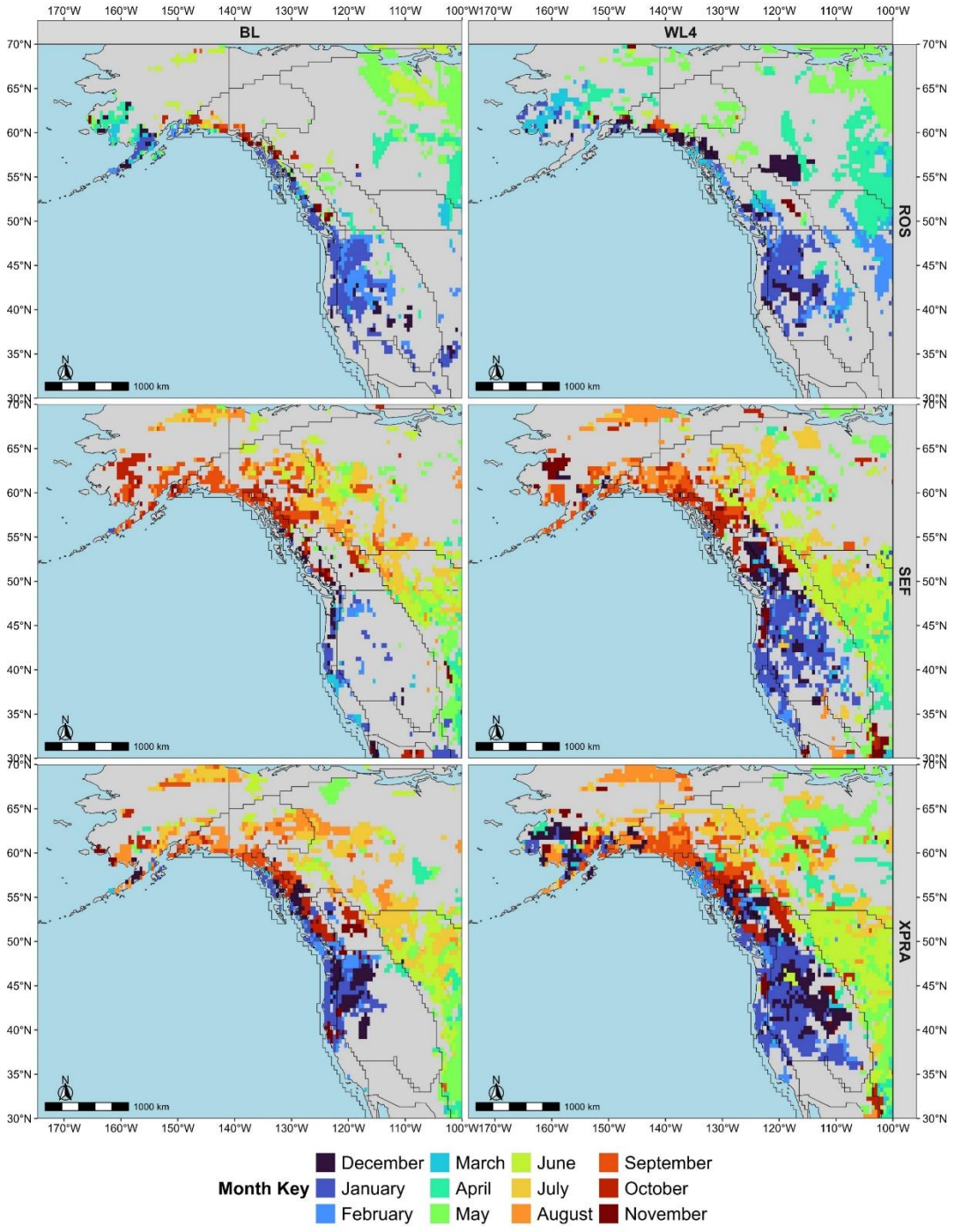

Figure 10: Spatial map showing the month with the highest ROS(top), SEF(middle) and XPRA(bottom) event magnitude in terms of runoff for each cell in the BL(left) and WL4(right) periods.

3.4 Influence of Internal Climate Variability

The role of internal climate variability in the projection of AR related CIF events is examined using the Signal to Noise Ratio (SNR). The SNR is calculated by dividing the change in mean probability of occurrence relative to the base line period for each warming level by the standard deviation across all model members. Then SNR is calculated for each cell in the model and plotted spatially in Figure 11. A projected SNR that is greater than (less than) 1 (-1) indicates a significant positive (negative) change in the probability of an event being AR related relative to the base line period. The results suggest that significant signals (SNR > 1 or < -1) are not prominent until the farthest warming scenario (WL4). Even at WL4, the results vary substantially between event types, and the spatial patterns are noisier compared to the probability of occurrence maps shown in Section 3.2, especially in the lower coastal areas. This means that earlier findings that ARs will play a larger role in extreme CIF and precipitation events contains a significant amount of uncertainty. These results align with previous findings suggesting that projected AR activity in climate models is dominated by internal climate variability (Gershunov, et al., 2019; Tseng et al., 2022). This is also reflected in the probability of occurrence maps with a decrease in statistically significant results relative to randomly generated conditions in later warming periods. One of the recurring patterns between scenarios is the formation of stronger positive signals within the MtWest region and other higher region areas. For example, the ROS results project a strong positive signal emerging in the highest elevation areas that can be identified in Figure 1 in later warming levels. This shows areas where projections have the highest certainty that AR contributions to CIF and extreme precipitation events will increase. This projection is likely strong since AR related precipitation is often generated through orthographic uplift. These results show that internal variability creates significant uncertainty in the context of AR related compound flooding events.

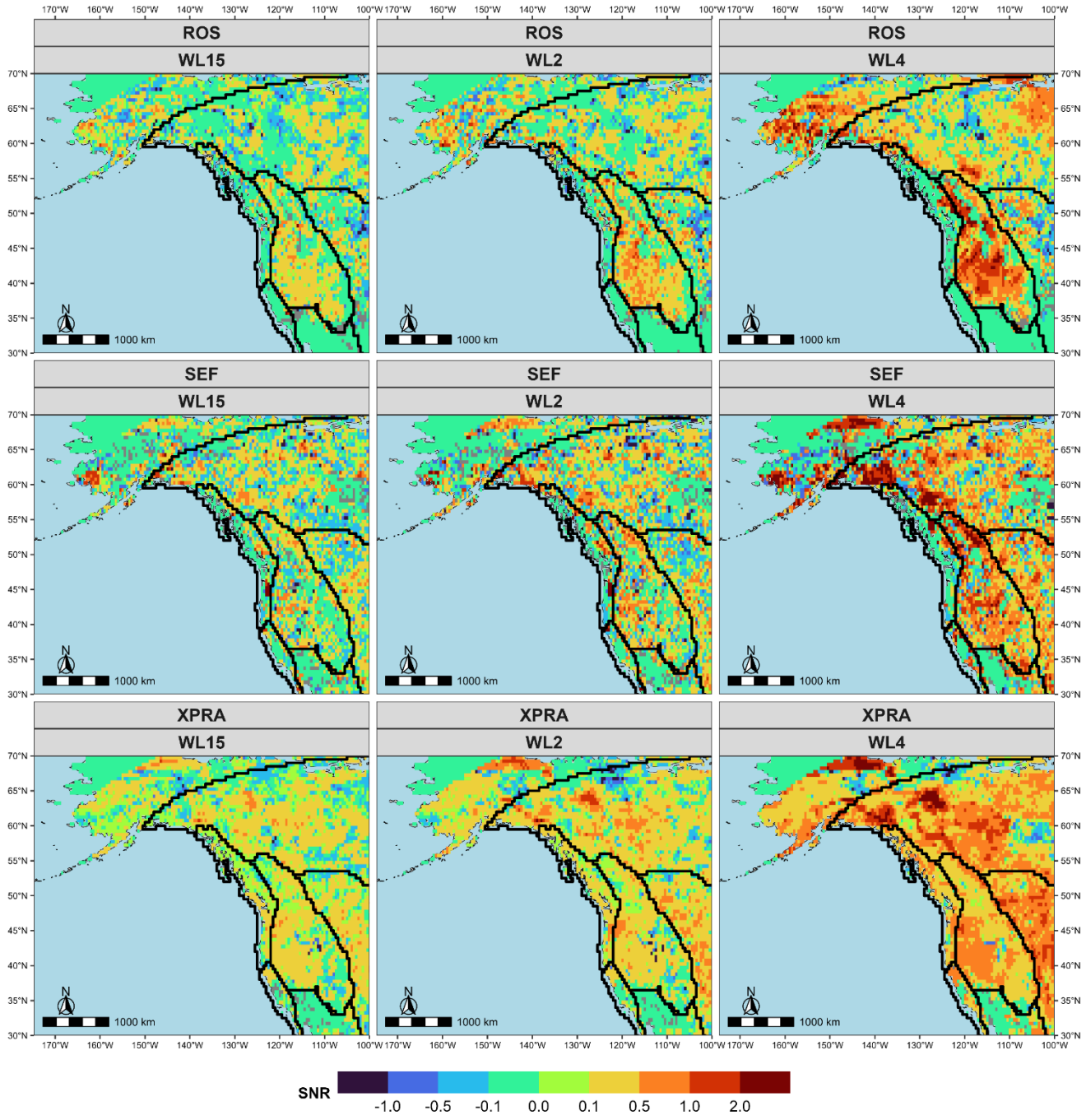

Figure 11: Signal to Noise Ratio for the probability that an event is AR related for each CIF event and extreme precipitation event. The SNR relative to the baseline period is shown for ROS, SEF and XPRA events in the top, middle and bottom rows respectively. Each column depicts a depicts a different warming level for each event, with the WL15, WL2, and WL4 being represented in the left, middle and right columns of plots respectively.

4. Discussion

4.1 AR and CIF Event Interactions in a Changing Climate

Investigation of the likelihood of AR contribution to events revealed that ARs are major contributors to extreme ROS and SEF events, especially in coastal and orthographic areas. This is highlighted when considering the overall likelihood of CIF events shown in Figure S3 which shows the areas with an increase in CIF likelihood generally see an increase in the likelihood of AR related events in Figure S2. Past studies in various places of North America also support that ARs disproportionately contribute to flooding events (Curry et al., 2019; Konrad and Dettinger, 2017; Nayak and Villarini, 2017). This relationship and its connection changing AR characteristics is explored in depth later in the discussion ARs contribute significantly less to overall extreme precipitation events compared to CIF events implying that AR related flooding is more dependent on pre-existing site conditions and not the characteristics of a landfalling AR. This argument is supported by case studies of past AR flooding events showing that weaker more commonly occurring ARs could be associated with catastrophic flooding conditions (Gillett et al., 2022; Konrad and Dettinger, 2017; Ralph et al., 2006). Another likely explanation for the results in this study is the increased amounts of ARs in the future will lead to an increase in temporally compounding atmospheric rivers. Temporally compounding ARs have been the subject of previous studies and would explain the high contribution of ARs to flooding events that require precipitation related antecedent conditions (Bowers et al., 2023, 2024; Fish et al., 2022). In theory an AR could make landfall and create wet conditions or build up snowpack. A subsequent AR arriving shortly afterward could then generate significant runoff by interacting with the recently saturated soil or accumulated snowpack.

The seasonality of joint AR and CIF occurrence seems to be determined by the regional and seasonal behavior of ARs. This means that in southern regions along the West Coast such as Northern California, AR related CIF events are more likely to occur in the winter. This is reflective of the seasonality commonly associated with ARs in the area (Gershunov et al., 2017; Ralph et al., 2013; Rutz et al., 2014). In higher latitudes like British Columbia or the Alaskan Coast, AR related events occur more in the fall or winter which is also consistent with past studies (Radić et al., 2015; Sharma and Déry, 2020a). This seasonality facilitates the occurrence of ROS, since ARs make landfall in colder season when there is more likely to be snowpack accumulated. Furthermore, in these regions the AR season occurs during the wet season which also promotes AR making landfall in areas with high soil moisture. The observed seasonality further supports the finding that most CIF events are strongly connected to AR activity. AR related ROS events, in particular, align with the seasonality of AR activity but are more concentrated in the winter period, as ROS events require a certain amount of accumulated snowpack to occur. This seasonal concentration is also reflected in the magnitude results. The observed patterns could be influenced by expected changes in North America's climate, where winters are projected to become shorter and warmer, reducing overall snowpack accumulation in many regions (Il Jeong and Sushama, 2018; IPCC, 2022; McCabe et al., 2007).

In a warmer climate, past studies showed that ARs are projected to become more frequent and severe (Espinoza et al., 2018; Gao et al., 2015; Radić et al., 2015; Shields and Kiehl, 2016). ARs are also projected to become warmer in temperature and are positively correlated with the warming of their area of origin (Gonzales et al., 2022). The increase in AR related CIF

magnitude and the likelihood of CIF events being driven by AR reflect these expected changes. Projections indicate that AR-related CIF events will generally become more frequent in a warmer climate, particularly during winter. However, for an AR to produce a high-magnitude CIF event, appropriate antecedent conditions, such as accumulated snowpack or saturated soils, are necessary. This is highlighted through a comparison of magnitudes generated by AR related XPRA events to the other CIF events. Although the CIF events are technically a subset of XPRA events, a strong connection with AR occurrence is only seen once criteria for antecedent conditions are included. Due to the highly regional and seasonal behaviour of ARs, the strong connection between extreme surface runoff and ARs could help further strengthen flood frequency models. Especially since numerous dams are in the areas that are projected to have the largest increases in AR related events. Furthermore, as a synoptic scale phenomenon, ARs can be modelled more easily than other CIF related mesoscale phenomena (Lavers et al., 2016). Since this relationship is also projected to strengthen in a warmer climate it could also be used as a basis for designing future infrastructure against severe flooding events.

4.2 Identified Relationships between ARs and CIF Events

The ROS projections generally follow projections reported in existing literature. ROS events are expected to become more frequent and severe in higher latitudes and elevations in future warming scenarios (Beniston and Stoffel, 2016; Il Jeong and Sushama, 2018; McCabe et al., 2007; Musselman et al., 2018). This is shown in the results through a projected increase in average runoff between BL and WL2 until a decrease in WL4. This observation is often attributed to a warmer climate that better facilitates the occurrence of rain during times when snowpack is present. Warmer ARs could further contribute to a reduction in the amount of snowpack since the average temperature of AR related snowfalls are already close to the freezing threshold, thus making them sensitive to changes in temperature (Gonzales et al., 2019, 2022; Guan et al., 2010). Although increased AR frequency promotes the occurrence of ROS events in a warmer climate there may be less snow on the ground to match this increase. One exception to this is during the winter in the PacificNW region where AR related ROS events are projected to become more frequent and intense in the furthest warming period. This reflects the discussed changes in ARs, which allow ROS events to occur in high elevation areas where snowpack is less affected by a warming climate. Past studies have found these areas are often projected to experience an increase in ROS events due to higher likelihood of liquid precipitation occurring during cold seasons in a warming climate (Beniston and Stoffel, 2016; McCabe et al., 2007; Warden et al., 2024). As shown in Section 3.3 this increase in frequency is what drives an apparent increase in projected runoff. The results of this study suggest that the occurrence of extreme ROS events could be facilitated by more frequent AR events in future winters. This is further supported by the probability of occurrence maps, which indicate that a substantial portion of ROS events in this region may be associated with AR activity. These findings imply that AR characteristics, such as frequency, temperature, and intensity, are likely important factors influencing present and future extreme ROS events.

Saturated soil conditions are known for exacerbating flooding conditions (Grillakis et al., 2016; Wasko et al., 2020); however, the results indicate that in a warmer climate a higher proportion of these events can be AR related. They further suggest that this will be likely driven by the large amounts of precipitation delivered by a landfalling AR relative to events without AR

influence. Currently there is a lack of literature that explicitly examines how ARs contribute to high soil moisture levels. A recent study suggests that ARs reduce evapotranspiration due to an increased cloud cover associated with ARs (Chen et al., 2019). This could explain why the results suggest a strong connection between ARs and SEF events. However, whether there is a direct connection between AR conditions and SEF events generating runoff remains an open question. A more likely explanation is that ARs are coinciding with high soil moisture retained from other events. Furthermore, there is also the increased occurrence of temporally occurring ARs making landfall discussed previously. Together this evidence suggests that temporally compounding AR events and hydrologic autocorrelation could drive the occurrence of SEF flooding, which is further supported by the results obtained for individual heavy rainfall events. The results indicate that a single AR associated with heavy precipitation is less likely to generate large amounts of runoff compared to SEF and ROS events. Additionally, there appears to be a potential connection between the decrease in ROS events and an increase in SEF events. This relationship may be driven by higher winter temperatures, which reduce snowmelt-driven runoff (ROS events) while increasing rainfall, thereby contributing to more SEF events.

4.3 Analysis of Uncertainties

The projected AR related CIF events in this study are associated with considerable uncertainty, primarily due to internal variability. This level of uncertainty is not unexpected, as previous studies have shown that AR activity, extreme events, and precipitation are often more effected by internal variability (Blanusa et al., 2023; Gershunov et al., 2019; Kelleher et al., 2023; Mahmoudi et al., 2021). AR activity is dictated by thermodynamic changes, such as rising temperatures, and dynamic changes, like changes in jet stream position (Gao et al., 2015; Zavadoff and Kirtman, 2020). Changes in AR frequency and magnitude are dominated by thermodynamic changes, however, changes in landfall location are more attributable to changes in dynamic drivers (Gao et al., 2015; Islam and Najafi, 2026; Tseng et al., 2022). Thermodynamic changes tend to exhibit stronger climate signals compared to dynamic changes, highlighting their dominant role in shaping AR characteristics under a warming climate (Deser et al., 2012). The established regional connection between AR occurrence and CIF events suggests that dynamic changes in AR behaviour, such as shifts in landfall location, may play a dominant role compared to thermodynamic changes in shaping AR-related CIF events. If common landfalling locations shift significantly under future warming scenarios, this could explain the difficulty in establishing a statistically robust relationship between ARs and CIF events in later warming periods, as such shifts are not explicitly accounted for in the current methodology. This highlights the need for further research to reduce uncertainties in modeling AR dynamics, which could improve projections of AR-related CIF events and their associated impacts under future climate scenarios (Gershunov, et al., 2019; Tseng et al., 2022). Increasing the number of members used in a model ensemble has been shown to better characterize the uncertainty related to internal variability in climate change studies (Deser, 2020; Deser et al., 2012; Fereshtehpour et al., 2025; Islam and Najafi, 2025; Na et al., 2025) especially in the context of compound events (Bevacqua et al., 2023). However, similar studies examining internal variability and ARs have had similar results despite having a higher number of members (Huang and Swain, 2022; Tseng et al., 2022) and compound inland flooding events have also been found to be strongly associated with internal variability (Fereshtehpour

et al., 2025). It is also important to note that significant uncertainty exists in the characterization of ARs themselves, largely due to the lack of consensus on how ARs should be defined as objects (Collow et al., 2022; Lora et al., 2020; Zhou et al., 2021). The existing literature highlights the substantial differences that can arise from the use of alternative AR detection methodologies (Ralph et al., 2019b; Rutz et al., 2019). Fully addressing the range of uncertainties identified here is beyond the scope of the present study and would require dedicated, in-depth investigations.

5. Conclusions

ARs have often been associated with catastrophic flooding events; however, past studies often focused on these events through a univariate lens by focusing on extreme precipitation or streamflow. Studies that do focus on AR interactions with preexisting conditions often overlook the potential impacts of climate change. The goal of this study was to quantify the extent to which CIF events can be attributed to ARs on the North American West Coast and assess how this relationship is projected to change under future climate scenarios. Using outputs from the CanRCM4-LE model, the analysis focused on calculating the projected contributions of ARs to CIF events, as well as the projected frequency and magnitudes of AR-driven CIF events. The results indicate that ARs are expected to play a growing role in the occurrence and severity of extreme ROS and SEF events. In contrast, ARs are found to have a less pronounced role in heavy rainfall events leading to the heavy runoff, highlighting the importance of antecedent conditions in AR related flooding events. This underscores the value of incorporating landfalling ARs within a compound event framework. In a warmer climate a majority of extreme ROS and SEF events may be associated with landfalling ARs. The seasonality of landfalling ARs, as identified in previous studies, complements and shapes the seasonality of AR-driven CIF events. The results regarding projected flooding risk and changes in CIF events align closely with past works and case studies.

To the authors knowledge, this work is among the first to investigate compound inland flooding driven by ARs and examine the combined influence of externally forced climate change and internal climate variability. These findings have implications for the prediction and analysis of future extreme runoff events and the design of critical infrastructure. Furthermore, they highlight that considering the impact of an AR by itself can underestimate its impact, and the role of in-situ conditions must be considered along with AR strength when considering potential impacts. The scope of this study excluded process-based models; however, future methodologies could incorporate such models at a smaller spatial scale to fully explore how ARs interact with other environmental drivers. While this study focuses on uncertainty associated with internal climate variability, other factors, such as dynamic processes, sample size, and AR detection methods, may also influence the results and warrant consideration in future research. Although these represent key uncertainties inherent to the problem, they fall outside the primary focus of this study and are therefore not fully characterized here. Nevertheless, the results presented here provide a foundation for future research specifically targeting the relationship between internal variability and AR-driven flooding, an important avenue underscored by the strong link identified between compound events and AR-related impacts. Future studies can improve the methodology by focusing on more characteristics of ARs such as specific AR intensity category and the role

of sequential ARs. Another potential area of future focus is a moisture budget-based analysis that focuses on the role of moisture convergence, convective mechanisms and other synoptic phenomena in the formation of extreme precipitation in the context of AR activity. This approach is supported by recently developed high-resolution regional moisture budget datasets (Raghuvanshi and Agarwal, 2025b, a). Reducing uncertainty in future analyses may involve accounting for potential dynamic changes in AR positioning and employing multiple AR detection methods to better quantify how much uncertainty is associated with the definition of an AR. By distinguishing the roles of internal variability and external forcing, this study establishes a critical framework for adapting flood risk management and infrastructure design to the intensifying AR-driven compound events.

Author Contribution

AG: Conceptualization, Data curation, Formal analysis, Investigation, Methodology, Software, Validation, Visualization, Writing – original draft; MF: Conceptualization, Data curation, Formal analysis, Investigation, Methodology, Writing – review & editing; MN: Conceptualization, Formal analysis, Investigation, Methodology, Software, Resources, Validation, Writing – review & editing, Funding acquisition, Project administration; AC: Data curation, Investigation, Writing – review & editing; HS: Investigation, Resources, Writing – review & editing..

Acknowledgments

This research was supported by Environment and Climate Change Canada (ECCC) through the Flood Hazard Identification and Mapping Program (Grant GCXE25M006).

Data Availability Statement

The data from the Canadian Regional Climate Model Large Ensemble (CanRCM4 LE) used in this study can be accessed on the Government of Canada Open Data Portal at: https://crd-data-donnees-rdc.ec.gc.ca/CCCMA/products/CanSISE/output/CCCma/CanRCM4/. The ERA5 reanalysis dataset used for validation in this study is available at the ECWMF climate data store which can be accessed at: https://cds.climate.copernicus.eu/datasets. The elevation data from the Global Multi-resolution Terrain Elevation Data 2010 can be accessed from the United States Geological Survey earth explorer data portal at https://earthexplorer.usgs.gov/. The Global Dam tracker data base can be found in cited paper within the manuscript or publicly available at https://zenodo.org/records/7616852.

References

Beniston, M. and Stoffel, M.: Rain-on-snow events, floods and climate change in the Alps: Events may increase with warming up to 4 °C and decrease thereafter, Sci. Total Environ., 571, 228–236, https://doi.org/10.1016/j.scitotenv.2016.07.146, 2016.

Bevacqua, E., Suarez-Gutierrez, L., Jézéquel, A., Lehner, F., Vrac, M., Yiou, P., and Zscheischler, J.: Advancing research on compound weather and climate events via large ensemble model simulations, Nat. Commun., 14, 2145, https://doi.org/10.1038/s41467-023-37847-5, 2023.

Blanusa, M. L., López-Zurita, C. J., and Rasp, S.: Internal variability plays a dominant role in global climate projections of temperature and precipitation extremes, Clim. Dyn., https://doi.org/10.1007/s00382-023-06664-3, 2023.

Bowers, C., Serafin, K. A., Tseng, K.-C., and Baker, J. W.: Atmospheric River Sequences as Indicators of Hydrologic Hazard in Historical Reanalysis and GFDL SPEAR Future Climate Projections, Earths Future, 11, e2023EF003536, https://doi.org/10.1029/2023EF003536, 2023.

Bowers, C., Serafin, K. A., and Baker, J. W.: Temporal compounding increases economic impacts of atmospheric rivers in California, Sci. Adv., 10, eadi7905, https://doi.org/10.1126/sciadv.adi7905, 2024.

Bukosvsky, M. S.: Masks for the Bukovsky regionalization of North America, 2011.

Cannon, A. J., Alford, H., Shrestha, R. R., Kirchmeier-Young, M. C., and Najafi, M. R.: Canadian Large Ensembles Adjusted Dataset version 1 (CanLEADv1): Multivariate bias-corrected climate model outputs for terrestrial modelling and attribution studies in North America, Geosci. Data J., 9, 288–303, https://doi.org/10.1002/gdj3.142, 2022.

Chen, X., Leung, L. R., Wigmosta, M., and Richmond, M.: Impact of Atmospheric Rivers on Surface Hydrological Processes in Western U.S. Watersheds, J. Geophys. Res. Atmospheres, 124, 8896–8916, https://doi.org/10.1029/2019JD030468, 2019.

Cobb, A., Delle Monache, L., Cannon, F., and Ralph, F. M.: Representation of Dropsonde-Observed Atmospheric River Conditions in Reanalyses, Geophys. Res. Lett., 48, e2021GL093357, https://doi.org/10.1029/2021GL093357, 2021.

Collow, A. B. M., Shields, C. A., Guan, B., Kim, S., Lora, J. M., McClenny, E. E., Nardi, K., Payne, A., Reid, K., Shearer, E. J., Tomé, R., Wille, J. D., Ramos, A. M., Gorodetskaya, I. V., Leung, L. R., O'Brien, T. A., Ralph, F. M., Rutz, J., Ullrich, P. A., and Wehner, M.: An Overview of ARTMIP's Tier 2 Reanalysis Intercomparison: Uncertainty in the Detection of Atmospheric Rivers and Their Associated Precipitation, J. Geophys. Res. Atmospheres, 127, e2021JD036155, https://doi.org/10.1029/2021JD036155, 2022.

Curry, C. L., Islam, S. U., Zwiers, F. W., and Déry, S. J.: Atmospheric Rivers Increase Future Flood Risk in Western Canada's Largest Pacific River, Geophys. Res. Lett., 46, 1651–1661, https://doi.org/10.1029/2018GL080720, 2019.

Danielson, J. and Gesch, D.: Global Multi-resolution Terrain Elevation Data 2010 (GMTED2010), U.S. Geological Survey, United States of America, 2011.

Deser, C.: "Certain Uncertainty: The Role of Internal Climate Variability in Projections of Regional Climate Change and Risk Management," Earths Future, 8, e2020EF001854, https://doi.org/10.1029/2020EF001854, 2020.

Deser, C., Phillips, A., Bourdette, V., and Teng, H.: Uncertainty in climate change projections: the role of internal variability, Clim. Dyn., 38, 527–546, https://doi.org/10.1007/s00382-010-0977-x, 2012.

Deser, C., Lehner, F., Rodgers, K. B., Ault, T., Delworth, T. L., DiNezio, P. N., Fiore, A., Frankignoul, C., Fyfe, J. C., Horton, D. E., Kay, J. E., Knutti, R., Lovenduski, N. S., Marotzke, J., McKinnon, K. A., Minobe, S., Randerson, J., Screen, J. A., Simpson, I. R., and Ting, M.: Insights from Earth system model initial-condition large ensembles and future prospects, Nat. Clim. Change, 10, 277–286, https://doi.org/10.1038/s41558-020-0731-2, 2020.

Espinoza, V., Waliser, D. E., Guan, B., Lavers, D. A., and Ralph, F. M.: Global Analysis of Climate Change Projection Effects on Atmospheric Rivers, Geophys. Res. Lett., 45, 4299–4308, https://doi.org/10.1029/2017GL076968, 2018.

Fereshtehpour, M., Najafi, M. R., and Cannon, A. J.: Characterizing Compound Inland Flooding Mechanisms and Risks in North America Under Climate Change, Earths Future, 13, e2024EF005353, https://doi.org/10.1029/2024EF005353, 2025.

Fereshtehpour M, Najafi MR, Leach JA, Wang Y. Quantifying the individual and combined influence of climate change, land cover transition, and internal climate variability on the hydrology of a snow-dominated forested watershed. Climatic Change. 2025 Feb;178(2):10.

Fish, M. A., Done, J. M., Swain, D. L., Wilson, A. M., Michaelis, A. C., Gibson, P. B., and Ralph, F. M.: Large-Scale Environments of Successive Atmospheric River Events Leading to Compound Precipitation Extremes in California, J. Clim., 35, 1515–1536, https://doi.org/10.1175/JCLI-D-21-0168.1, 2022.

Freudiger, D., Kohn, I., Stahl, K., and Weiler, M.: Large-scale analysis of changing frequencies of rain-on-snow events with flood-generation potential, Hydrol. Earth Syst. Sci., 18, 2695–2709, https://doi.org/10.5194/hess-18-2695-2014, 2014.

Gao, Y., Lu, J., Leung, L. R., Yang, Q., Hagos, S., and Qian, Y.: Dynamical and thermodynamical modulations on future changes of landfalling atmospheric rivers over western North America, Geophys. Res. Lett., 42, 7179–7186, https://doi.org/10.1002/2015GL065435, 2015.

Gershunov, A., Shulgina, T., Ralph, F. M., Lavers, D. A., and Rutz, J. J.: Assessing the climate-scale variability of atmospheric rivers affecting western North America, Geophys. Res. Lett., 44, 7900–7908, https://doi.org/10.1002/2017GL074175, 2017.

Gershunov, A., Shulgina, T., Clemesha, R. E. S., Guirguis, K., Pierce, D. W., Dettinger, M. D., Lavers, D. A., Cayan, D. R., Polade, S. D., Kalansky, J., and Ralph, F. M.: Precipitation regime change in Western North America: The role of Atmospheric Rivers, Sci. Rep., 9, 9944, https://doi.org/10.1038/s41598-019-46169-w, 2019.

Gillett, N. P., Cannon, A. J., Malinina, E., Schnorbus, M., Anslow, F., Sun, Q., Kirchmeier-Young, M., Zwiers, F., Seiler, C., Zhang, X., Flato, G., Wan, H., Li, G., and Castellan, A.: Human influence on the 2021 British Columbia floods, Weather Clim. Extrem., 36, 100441, https://doi.org/10.1016/j.wace.2022.100441, 2022.

Gonzales, K. R., Swain, D. L., Nardi, K. M., Barnes, E. A., and Diffenbaugh, N. S.: Recent Warming of Landfalling Atmospheric Rivers Along the West Coast of the United States, J. Geophys. Res. Atmospheres, 124, 6810–6826, https://doi.org/10.1029/2018JD029860, 2019.

Gonzales, K. R., Swain, D. L., Roop, H. A., and Diffenbaugh, N. S.: Quantifying the Relationship Between Atmospheric River Origin Conditions and Landfall Temperature, J. Geophys. Res. Atmospheres, 127, e2022JD037284, https://doi.org/10.1029/2022JD037284, 2022.

Grillakis, M. G., Koutroulis, A. G., Komma, J., Tsanis, I. K., Wagner, W., and Blöschl, G.: Initial soil moisture effects on flash flood generation – A comparison between basins of contrasting hydro-climatic conditions, J. Hydrol., 541, 206–217, https://doi.org/10.1016/j.jhydrol.2016.03.007, 2016.

Guan, B. and Waliser, D. E.: Detection of atmospheric rivers: Evaluation and application of an algorithm for global studies, J. Geophys. Res. Atmospheres, 120, 12514–12535, https://doi.org/10.1002/2015JD024257, 2015.

Guan, B. and Waliser, D. E.: Tracking Atmospheric Rivers Globally: Spatial Distributions and Temporal Evolution of Life Cycle Characteristics, J. Geophys. Res. Atmospheres, 124, 12523–12552, https://doi.org/10.1029/2019JD031205, 2019.

Guan, B., Molotch, N. P., Waliser, D. E., Fetzer, E. J., and Neiman, P. J.: Extreme snowfall events linked to atmospheric rivers and surface air temperature via satellite measurements, Geophys. Res. Lett., 37, https://doi.org/10.1029/2010GL044696, 2010.

Guan, B., Waliser, D. E., and Ralph, F. M.: Global Application of the Atmospheric River Scale, J. Geophys. Res. Atmospheres, 128, e2022JD037180, https://doi.org/10.1029/2022JD037180, 2023.

Hagos, S. M., Leung, L. R., Yoon, J.-H., Lu, J., and Gao, Y.: A projection of changes in landfalling atmospheric river frequency and extreme precipitation over western North America from the Large Ensemble CESM simulations, Geophys. Res. Lett., 43, 1357–1363, https://doi.org/10.1002/2015GL067392, 2016.

Hersbach, H., Bell, B., Berrisford, P., Hirahara, S., Horányi, A., Muñoz-Sabater, J., Nicolas, J., Peubey, C., Radu, R., Schepers, D., Simmons, A., Soci, C., Abdalla, S., Abellan, X., Balsamo, G., Bechtold, P., Biavati, G., Bidlot, J., Bonavita, M., De Chiara, G., Dahlgren, P., Dee, D., Diamantakis, M., Dragani, R., Flemming, J., Forbes, R., Fuentes, M., Geer, A., Haimberger, L., Healy, S., Hogan, R. J., Hólm, E., Janisková, M., Keeley, S., Laloyaux, P., Lopez, P., Lupu, C., Radnoti, G., de Rosnay, P., Rozum, I., Vamborg, F., Villaume, S., and Thépaut, J.-N.: The ERA5 global reanalysis, Q. J. R. Meteorol. Soc., 146, 1999–2049, https://doi.org/10.1002/qj.3803, 2020.

Huang, X. and Swain, D. L.: Climate change is increasing the risk of a California megaflood, Sci. Adv., 8, eabq0995, https://doi.org/10.1126/sciadv.abq0995, 2022.

Il Jeong, D. and Cannon, A. J.: Projected changes to risk of wind-driven rain on buildings in Canada under +0.5 °C to +3.5 °C global warming above the recent period, Clim. Risk Manag., 30, 100261, https://doi.org/10.1016/j.crm.2020.100261, 2020.

Il Jeong, D. and Sushama, L.: Rain-on-snow events over North America based on two Canadian regional climate models, Clim. Dyn., 50, 303–316, https://doi.org/10.1007/s00382-017-3609-x, 2018.

IPCC: Climate Change 2022: Impacts, Adaptation, and Vulnerability. Contribution of Working Group II to the SIxth Assessment Report of the Intergovernmental Panel on Climate Change, edited by: Pörtner, H.-O., Roberts, D. C., Tignor, M., Poloczanska, E. S., Mintenbeck, K., Alegria, A., Craig, M., Langsdorf, S., Löschke, S., Möller, V., Okem, A., and Rama, B., Cambridge University Press, Cambridge, UK and New York, NY, USA, 3056 pp., 2022.

Islam MR, Najafi MR. Dynamic and thermodynamic drivers of extreme precipitation under nonstationarity: implications for probable maximum precipitation across North America. Natural Hazards. 2026 Jan;122(1):39.

Islam MR, Najafi MR. Machine learning-based regional flood frequency framework for climate resilient infrastructure. Journal of Hydrology. 2025 Jun 14:133703.

Kay, J. E., Deser, C., Phillips, A., Mai, A., Hannay, C., Strand, G., Arblaster, J. M., Bates, S. C., Danabasoglu, G., Edwards, J., Holland, M., Kushner, P., Lamarque, J.-F., Lawrence, D., Lindsay, K., Middleton, A., Munoz, E., Neale, R., Oleson, K., Polvani, L., and Vertenstein, M.: The Community Earth System Model (CESM) Large Ensemble Project: A Community Resource for Studying Climate Change in the Presence of Internal Climate Variability, Bull. Am. Meteorol. Soc., 96, 1333–1349, https://doi.org/10.1175/BAMS-D-13-00255.1, 2015.

Kelleher, M. K., Grise, K. M., and Schmidt, D. F.: Variability in Projected North American Mean and Extreme Temperature and Precipitation Trends for the 21st Century: Model-To-Model Differences Versus Internal Variability, Earths Future, 11, e2022EF003161, https://doi.org/10.1029/2022EF003161, 2023.

Konrad, C. P. and Dettinger, M. D.: Flood Runoff in Relation to Water Vapor Transport by Atmospheric Rivers Over the Western United States, 1949–2015, Geophys. Res. Lett., 44, 11,456-11,462, https://doi.org/10.1002/2017GL075399, 2017.

Lavers, D. A. and Villarini, G.: The contribution of atmospheric rivers to precipitation in Europe and the United States, J. Hydrol., 522, 382–390, https://doi.org/10.1016/j.jhydrol.2014.12.010, 2015.

Lavers, D. A., Waliser, D. E., Ralph, F. M., and Dettinger, M. D.: Predictability of horizontal water vapor transport relative to precipitation: Enhancing situational awareness for forecasting western U.S. extreme precipitation and flooding, Geophys. Res. Lett., 43, 2275–2282, https://doi.org/10.1002/2016GL067765, 2016.

Lora, J. M., Shields, C. A., and Rutz, J. J.: Consensus and Disagreement in Atmospheric River Detection: ARTMIP Global Catalogues, Geophys. Res. Lett., 47, e2020GL089302, https://doi.org/10.1029/2020GL089302, 2020.

Ma, W., Chen, G., Guan, B., Shields, C. A., Tian, B., and Yanez, E.: Evaluating the Representations of Atmospheric Rivers and Their Associated Precipitation in Reanalyses With Satellite Observations, J. Geophys. Res. Atmospheres, 128, e2023JD038937, https://doi.org/10.1029/2023JD038937, 2023.

Mahmoudi, M. H., Najafi, M. R., Singh, H., and Schnorbus, M.: Spatial and temporal changes in climate extremes over northwestern North America: the influence of internal climate variability and external forcing, Clim. Change, 165, 14, https://doi.org/10.1007/s10584-021-03037-9, 2021.

McCabe, G. J., Clark, M. P., and Hay, L. E.: Rain-on-Snow Events in the Western United States, Bull. Am. Meteorol. Soc., 88, 319–328, https://doi.org/10.1175/BAMS-88-3-319, 2007.

Michaelis, A. C., Gershunov, A., Weyant, A., Fish, M. A., Shulgina, T., and Ralph, F. M.: Atmospheric River Precipitation Enhanced by Climate Change: A Case Study of the Storm That Contributed to California's Oroville Dam Crisis, Earths Future, 10, e2021EF002537, https://doi.org/10.1029/2021EF002537, 2022.

Mishra, A. N., Maraun, D., Schiemann, R., Hodges, K., Zappa, G., and Ossó, A.: Long-lasting intense cut-off lows to become more frequent in the Northern Hemisphere, Commun. Earth Environ., 6, 115, https://doi.org/10.1038/s43247-025-02078-7, 2025.

Mo, R., So, R., Brugman, M. M., Mooney, C., Liu, A. Q., Jakob, M., Castellan, A., and Vingarzan, R.: Column Relative Humidity and Primary Condensation Rate as Two Useful Supplements to Atmospheric River Analysis, Water Resour. Res., 57, e2021WR029678, https://doi.org/10.1029/2021WR029678, 2021.

Musselman, K. N., Lehner, F., Ikeda, K., Clark, M. P., Prein, A. F., Liu, C., Barlage, M., and Rasmussen, R.: Projected increases and shifts in rain-on-snow flood risk over western North America, Nat. Clim. Change, 8, 808–812, https://doi.org/10.1038/s41558-018-0236-4, 2018.

Na W, Grgas-Svirac AV, Najafi MR. Intensifying hydroclimatic swings under a warming climate: Disentangling anthropogenic climate change and internal variability in North America. Global and Planetary Change. 2025 Nov 8:105171.

Nayak, M. A. and Villarini, G.: A long-term perspective of the hydroclimatological impacts of atmospheric rivers over the central United States, Water Resour. Res., 53, 1144–1166, https://doi.org/10.1002/2016WR019033, 2017.

Oakley, N. S., Lancaster, J. T., Kaplan, M. L., and Ralph, F. M.: Synoptic conditions associated with cool season post-fire debris flows in the Transverse Ranges of southern California, Nat. Hazards, 88, 327–354, https://doi.org/10.1007/s11069-017-2867-6, 2017.

Poschlod, B., Zscheischler, J., Sillmann, J., Wood, R. R., and Ludwig, R.: Climate change effects on hydrometeorological compound events over southern Norway, Weather Clim. Extrem., 28, 100253, https://doi.org/10.1016/j.wace.2020.100253, 2020.

Radić, V., Cannon, A. J., Menounos, B., and Gi, N.: Future changes in autumn atmospheric river events in British Columbia, Canada, as projected by CMIP5 global climate models, J. Geophys. Res. Atmospheres, 120, 9279–9302, https://doi.org/10.1002/2015JD023279, 2015.

Raghuvanshi, A. S. and Agarwal, A.: An Hourly Dataset of Moisture Budget Components Over the Indian Subcontinent (1940–2024), Sci. Data, 12, 1770, https://doi.org/10.1038/s41597-025-06044-y, 2025a.

Raghuvanshi, A. S. and Agarwal, A.: Complex network reveals propagation and moisture dynamics of Indian monsoon precipitation extremes, Clim. Dyn., 63, 443, https://doi.org/10.1007/s00382-025-07924-0, 2025b.

Ralph, F. M., Neiman, P. J., Wick, G. A., Gutman, S. I., Dettinger, M. D., Cayan, D. R., and White, A. B.: Flooding on California's Russian River: Role of atmospheric rivers, Geophys. Res. Lett., 33, https://doi.org/10.1029/2006GL026689, 2006.

Ralph, F. M., Coleman, T., Neiman, P. J., Zamora, R. J., and Dettinger, M. D.: Observed Impacts of Duration and Seasonality of Atmospheric-River Landfalls on Soil Moisture and Runoff in Coastal Northern California, J. Hydrometeorol., 14, 443–459, https://doi.org/10.1175/JHM-D-12-076.1, 2013.

Ralph, F. M., Rutz, J. J., Cordeira, J. M., Dettinger, M., Anderson, M., Reynolds, D., Schick, L. J., and Smallcomb, C.: A Scale to Characterize the Strength and Impacts of Atmospheric Rivers, Bull. Am. Meteorol. Soc., 100, 269–289, https://doi.org/10.1175/BAMS-D-18-0023.1, 2019a.

Ralph, F. M., Wilson, A. M., Shulgina, T., Kawzenuk, B., Sellars, S., Rutz, J. J., Lamjiri, M. A., Barnes, E. A., Gershunov, A., Guan, B., Nardi, K. M., Osborne, T., and Wick, G. A.: ARTMIP-early start comparison of atmospheric river detection tools: how many atmospheric rivers hit northern California's Russian River watershed?, Clim. Dyn., 52, 4973–4994, https://doi.org/10.1007/s00382-018-4427-5, 2019b.

Ridder, N., de Vries, H., and Drijfhout, S.: The role of atmospheric rivers in compound events consisting of heavy precipitation and high storm surges along the Dutch coast, Nat. Hazards Earth Syst. Sci., 18, 3311–3326, https://doi.org/10.5194/nhess-18-3311-2018, 2018.

Rutz, J. J., Steenburgh, W. J., and Ralph, F. M.: Climatological Characteristics of Atmospheric Rivers and Their Inland Penetration over the Western United States, Mon. Weather Rev., 142, 905–921, https://doi.org/10.1175/MWR-D-13-00168.1, 2014.

Rutz, J. J., Steenburgh, W. J., and Ralph, F. M.: The Inland Penetration of Atmospheric Rivers over Western North America: A Lagrangian Analysis, Mon. Weather Rev., 143, 1924–1944, https://doi.org/10.1175/MWR-D-14-00288.1, 2015.

Rutz, J. J., Shields, C. A., Lora, J. M., Payne, A. E., Guan, B., Ullrich, P., O'Brien, T., Leung, L. R., Ralph, F. M., Wehner, M., Brands, S., Collow, A., Goldenson, N., Gorodetskaya, I., Griffith, H., Kashinath, K., Kawzenuk, B., Krishnan, H., Kurlin, V., Lavers, D., Magnusdottir, G., Mahoney, K., McClenny, E., Muszynski, G., Nguyen, P. D., Prabhat, Mr., Qian, Y., Ramos, A. M., Sarangi, C., Sellars, S., Shulgina, T., Tome, R., Waliser, D., Walton, D., Wick, G., Wilson, A. M., and Viale, M.: The

Atmospheric River Tracking Method Intercomparison Project (ARTMIP): Quantifying Uncertainties in Atmospheric River Climatology, J. Geophys. Res. Atmospheres, 124, 13777–13802, https://doi.org/10.1029/2019JD030936, 2019.

Scinocca, J. F., Kharin, V. V., Jiao, Y., Qian, M. W., Lazare, M., Solheim, L., Flato, G. M., Biner, S., Desgagne, M., and Dugas, B.: Coordinated Global and Regional Climate Modeling, J. Clim., 29, 17–35, https://doi.org/10.1175/JCLI-D-15-0161.1, 2016.

Sharma, A. R. and Déry, S. J.: Contribution of Atmospheric Rivers to Annual, Seasonal, and Extreme Precipitation Across British Columbia and Southeastern Alaska, J. Geophys. Res. Atmospheres, 125, e2019JD031823, https://doi.org/10.1029/2019JD031823, 2020a.

Sharma, A. R. and Déry, S. J.: Linking Atmospheric Rivers to Annual and Extreme River Runoff in British Columbia and Southeastern Alaska, J. Hydrometeorol., 21, 2457–2472, https://doi.org/10.1175/JHM-D-19-0281.1, 2020b.

Shields, C. A. and Kiehl, J. T.: Atmospheric river landfall-latitude changes in future climate simulations, Geophys. Res. Lett., 43, 8775–8782, https://doi.org/10.1002/2016GL070470, 2016.

Singh, H., Najafi, M. R., and Cannon, A. J.: Characterizing non-stationary compound extreme events in a changing climate based on large-ensemble climate simulations., Clim. Dyn., 56, 1389–1406, https://doi.org/10.1007/s00382-020-05538-2, 2021.

Tseng, K.-C., Johnson, N. C., Kapnick, S. B., Cooke, W., Delworth, T. L., Jia, L., Lu, F., McHugh, C., Murakami, H., Rosati, A. J., Wittenberg, A. T., Yang, X., Zeng, F., and Zhang, L.: When Will Humanity Notice Its Influence on Atmospheric Rivers?, J. Geophys. Res. Atmospheres, 127, e2021JD036044, https://doi.org/10.1029/2021JD036044, 2022.

Ullrich, P. A., Zarzycki, C. M., McClenny, E. E., Pinheiro, M. C., Stansfield, A. M., and Reed, K. A.: TempestExtremes v2.1: a community framework for feature detection, tracking, and analysis in large datasets, Geosci. Model Dev., 14, 5023–5048, https://doi.org/10.5194/gmd-14-5023-2021, 2021.

Warden, J. W., Rezvani, R., Najafi, M. R., and Shrestha, R. R.: Projections of rain-on-snow events in a sub-arctic river basin under 1.5°C–4°C global warming, Hydrol. Process., 38, e15250, https://doi.org/10.1002/hyp.15250, 2024.

Wasko, C., Nathan, R., and Peel, M. C.: Changes in Antecedent Soil Moisture Modulate Flood Seasonality in a Changing Climate, Water Resour. Res., 56, e2019WR026300, https://doi.org/10.1029/2019WR026300, 2020.

Whan, K. and Zwiers, F.: Evaluation of extreme rainfall and temperature over North America in CanRCM4 and CRCM5, Clim. Dyn., 46, 3821–3843, https://doi.org/10.1007/s00382-015-2807-7, 2016.

Wilks, D. S.: "The Stippling Shows Statistically Significant Grid Points": How Research Results are Routinely Overstated and Overinterpreted, and What to Do about It, Bull. Am. Meteorol. Soc., 97, 2263–2273, https://doi.org/10.1175/BAMS-D-15-00267.1, 2016.

Zavadoff, B. L. and Kirtman, B. P.: Dynamic and Thermodynamic Modulators of European Atmospheric Rivers, J. Clim., 33, 4167–4185, https://doi.org/10.1175/JCLI-D-19-0601.1, 2020.

Zhang, A. T. and Gu, V. X.: Global Dam Tracker: A database of more than 35,000 dams with location, catchment, and attribute information, Sci. Data, 10, 111, https://doi.org/10.1038/s41597-023-02008-2, 2023.

Zhou, Y., O'Brien, T. A., Ullrich, P. A., Collins, W. D., Patricola, C. M., and Rhoades, A. M.: Uncertainties in Atmospheric River Lifecycles by Detection Algorithms: Climatology and Variability, J. Geophys. Res. Atmospheres, 126, e2020JD033711, https://doi.org/10.1029/2020JD033711, 2021.